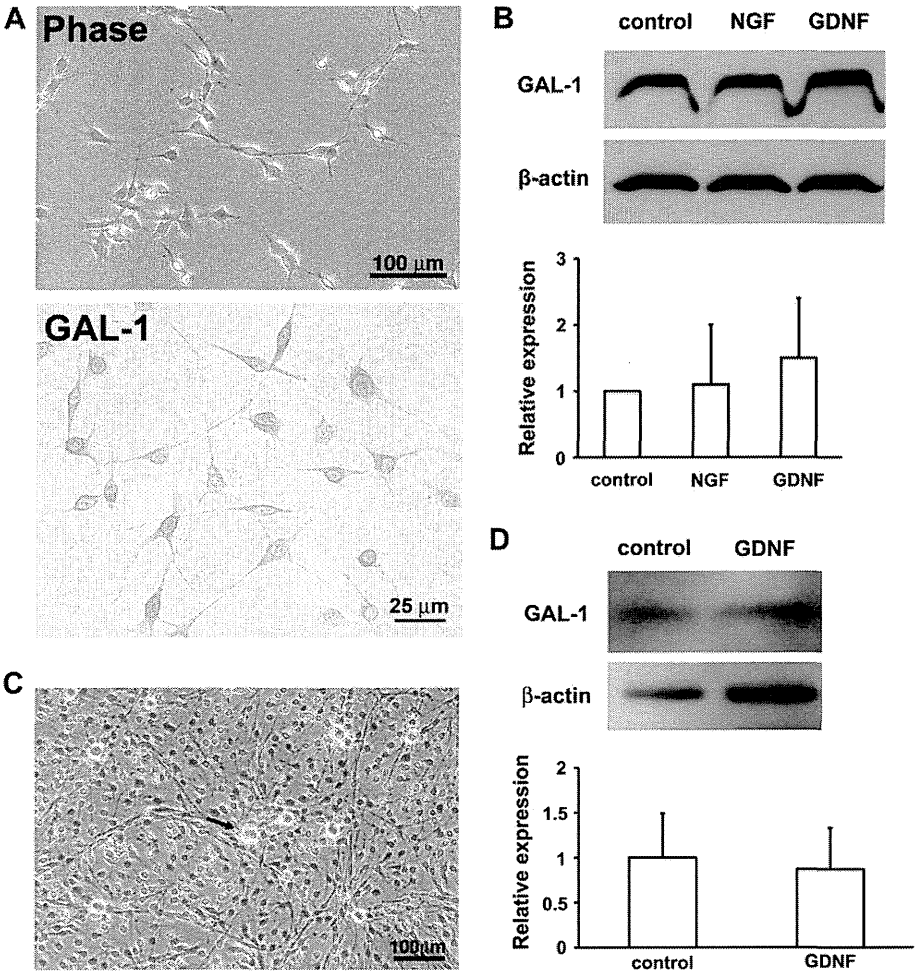

Fig. 3. GDNF fails to upregulate the expression of GAL-1 in immortalized Schwann cells IFRS1 and DRG neuron-IFRS1 cocultures. (A) A phase-contrast micrograph of IFRS1 cells (Left) and immunocytochemical localization of GAL-1 (Right). (B) The protein expression of GAL-1 in NGF- and GDNF-treated cells relative to that in untreated cells (control). Values represent the means and SD of 4 experiments. (C) A phase-contrast micrograph of DRG neurons (indicated as arrows) cocultured with IFRS1 cells. (D) The protein expression of GAL-1 in GDNF-treated cells relative to that in untreated cells (control). Values represent the means and SD of 4 experiments.

(McGraw et al., 2005b), which finding indicates the involvement of GAL-1 in the proper phenotypic differentiation of the non-peptidergic neurons.

Since density gradient centrifugation with 30% Percoll increases the neuronal yield and purity up to 90% (Goldenberg and De Boni, 1983), we have applied this method to the neurite outgrowth assays and Western blot analysis (Sango et al., 2008). However, it is inevitable that a small number of non-neuronal cells (*e.g.*, Schwann cells, fibroblasts, and perineurial cells) remain in the neuron-enriched solution (Sango et al., 2011). The maintenance of the culture in serum-free conditions inhibited the proliferation of these non-neuronal cells, but failed to completely eliminate them from the culture. Since GAL-1 has been shown to be highly expressed in DRG neurons and Schwann cells both *in vivo* and *in vitro* (Fukaya et al., 2003; Sango et al., 2004) and GDNF-mediated signaling pathways in cultured Schwann cells have been investigated (Paratcha et al., 2003; Iwase et al., 2005), we cannot deny the possibility that GDNF acts on Schwann cells to upregulate GAL-1 expression. To avoid the time-consuming process for getting good yields of primary cultured Schwann cells with high purity, we employed spontaneously immortalized Schwann cells IFRS1 for Western blot analysis. IFRS1 cells have been established from long-term cultures of adult rat DRG and peripheral nerves (Sango et al., 2011). These cells retain the characteristic features of mature Schwann cells as described in Results, and the ability to myelinate neurites in coculture with primary cultured and lined neurons has significant advantages for the study of peripheral nerve degeneration and regeneration, as compared to other Schwann cell lines (*e.g.* IMS32 (Watabe et al., 1995; Sango et al., 2004)). Western blot and immunocytochemical analyses on IFRS1 cells revealed intense immunoreactivity for GAL-1 (Sango et al., 2012a), which was not augmented by NGF or GDNF. Hence, it appears that GDNF upregulates GAL-1 expression in DRG culture through acing on neurons, rather than Schwann cells. This idea is supported by different GDNF signaling molecules and pathways between neurons and Schwann cells (Airaksinen and Saarma, 2002; Paratcha et al., 2003). It is also noteworthy that the growing body of evidence indicates the role of GAL-1 in the pathobiology of glial cells (Qu et al., 2011; Kurihara et al., 2010; Starossom et al., 2012) and neuron–glia interactions (Yamane et al., 2010; Stancic et al., 2011). GDNF has been shown to promote myelination in coculture of DRG neurons and IFRS1 cells (Sango et al., 2011), but it failed to upregulate GAL-1 in the same coculture system in this study. In addition, we previously showed that GDNF promoted the neurite outgrowth but not the viability of cultured DRG neurons (Sango et al., 2008). Although further study is needed, the GDNF/GAL-1 signaling axis shown in this study appears to be more involved in initial axonal regeneration, rather than neuroprotection and remyelination during the repair process after peripheral nerve injury.

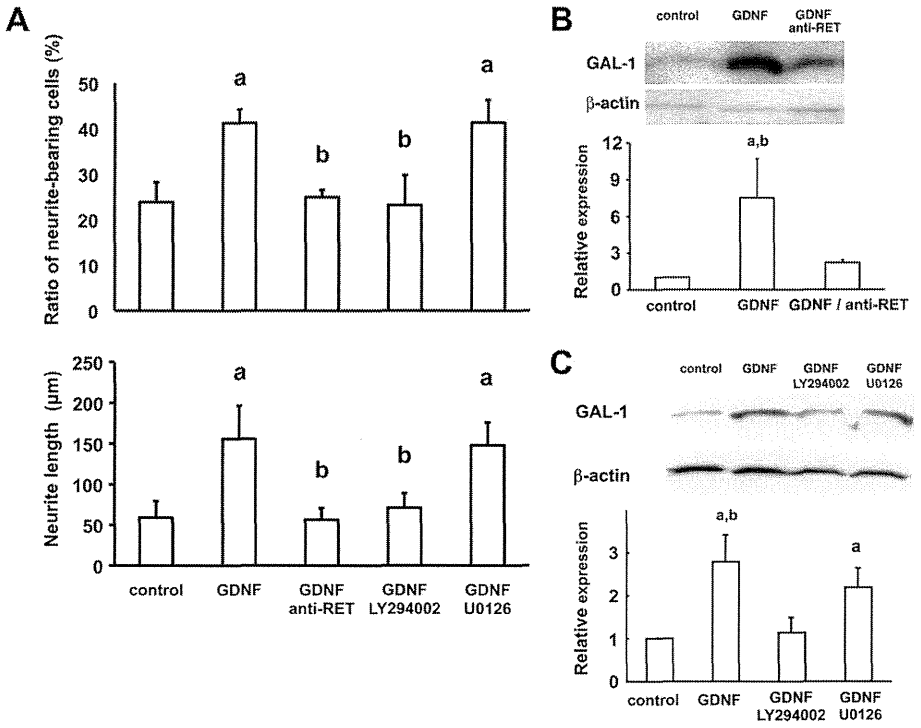

Fig. 4. Involvement of the RET/PI3K signaling pathway in GDNF-induced neurite outgrowth and upregulation of GAL-1 expression in DRG neurons. (A) Effects of the anti-RET antibody (H-300; Santa Cruz Biotech, 2 μg/ml), the PI3K inhibitor LY294002 (25 μM), and the MAPK kinase inhibitor U0126 (25 μM), on the ratios of neurite-bearing cells (upper) and the neurite length (lower) after 2 days in culture in the presence of GDNF (50 ng/ml). Values represent the means and SD of 5–8 experiments with 9 animals. a: $P < 0.05$ as compared with control, b: $P < 0.05$ as compared with GDNF. (B) Effects of the anti-RET on the GAL-1 expression after 2 days in culture in the presence of GDNF (Western blot analysis). Values represent the means and SD of 3 experiments with 9 animals. a: $P < 0.05$ as compared with control, b: $P < 0.05$ as compared with GDNF /anti-RET. (C) Effects of LY294002 (25 μM) and U0126 (25 μM) on the expression of GAL-1 after 2 days in culture in the presence of GDNF. Values represent the means and SD of 4 experiments with 12 animals. a: $P < 0.05$ as compared with control, b: $P < 0.05$ as compared with GDNF/LY294002.

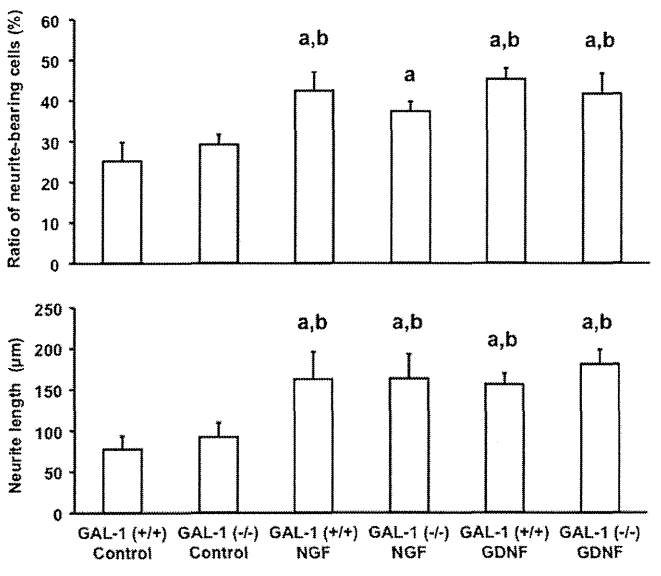

Fig. 5. DRG neurons from GAL-1 knockout mice (GAL-1 (−/−)) show similar neurite outgrowth activities to those from wild-type mice (GAL-1 (+/+)), in the presence or absence of NGF or GDNF. Values represent the means and SD of 3–6 experiments with 3 individuals in each group of mice. a: $P < 0.05$ as compared with GAL-1 (+/+) control, b: $P < 0.05$ as compared with GAL-1 (−/−) control.

A further question that arises here is which subpopulation of cultured DRG neurons contributes to the upregulation of GAL-1 in response to GDNF. We (Sango et al., 2012a) and others (Imbe et al., 2003) observed the predominant expression of GAL-1 in small IB4-binding DRG neurons *in vivo*. In addition, Gavazzi et al. (1999) reported that GDNF promoted neurite outgrowth from IB4-positive DRG neurons to a greater extent than NGF. Since GDNF-induced upregulation of GAL-1 was synchronized with acceleration of neurite outgrowth in this study, it seems reasonable to suppose that small IB4-binding neurons are major target cells of GDNF. Moreover, GDNF increased the ratios of IB4-binding neurons in culture, which finding agrees with those in a previous study that axotomy-induced downregulation of IB4-binding was restored by intrathecal administration of GDNF (Bennett et al., 1998). These findings suggest a role of GDNF in the maintenance of the non-peptidergic neuron phenotype after axonal injury. However, the intense GAL-1 immunoreactivity in both small and large neurons in culture in the presence or absence of GDNF (Sango et al., 2004, 2012a) is in contrast to the small neuron-predominant expression *in vivo*. Since enzymatic and mechanical treatments for the dissociation of DRG cells together with disruption of interactions between neurons and non-neuronal cells are detrimental to neurons, GAL-1 expressed in almost all neurons may function as a stress marker protein (Iwamoto et al., 2010) and/or a cytoprotective molecule (Lekishvili et al., 2006). Besides such ubiquitous GAL-1 induction during *in vivo–in vitro* replacement, GDNF may restore small neurons to the IB4-binding phenotype and upregulate GAL-1 expression in those cells. The Western blot analysis, but not the immunocytochemistry, demonstrated further increase in GAL-1 levels following GDNF treatment in this study. This may be due to intense histochemical expression of GAL-1 in cultured DRG neurons as described above and/or high sensitivity of the anti-GAL-1 antibody (Horie et al., 1999). We diluted the antibody up to 1:5000, but failed to show clear differences in the staining intensity between GDNF-treated and control DRG neurons (not shown). As long as the GAL-1 antibody is used, Western blot analysis is more accurate and suitable for the quantitative study than

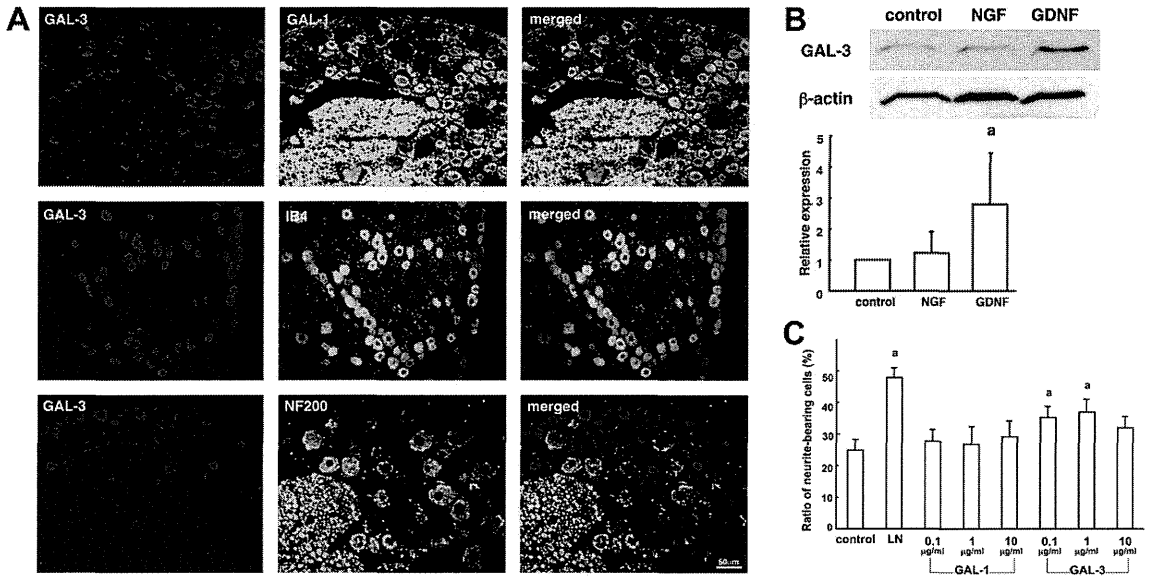

Fig. 6. GAL-3 appears to be involved in GDNF-induced neurite outgrowth. (A) Immunofluorescence micrographs of adult rat DRG sections, stained with antibodies to GAL-3 (red) and GAL-1, IB4, or NF200 (green). Note that most of the GAL-3-rich neurons are intensely stained with GAL-1 and IB4, but not with NF200. (B) GDNF upregulates GAL-3 expression in DRG cells. (Upper) Representative Western blot; the blotting for GAL-1, GAL-3, and β-actin are carried out at the same time (Fig. 2). The expression band of GAL-3 is identified as the level a molecular size of around 30 kDa. (Lower) The protein expression of GAL-3 in NGF- and GDNF-treated cells relative to that in untreated cells (control). Values represent the means and SD of 3–4 experiments with 12 animals. a: $P < 0.05$ as compared with control. (C) Recombinant GAL-3 used as a coating substratum promotes DRG neurite outgrowth, whereas recombinant GAl-1 has no bioactivities. Values represent the means and SD of 3–6 experiments with 3 rats. a: $P < 0.05$ as compared with control.

immunohistochemistry. The large error bars in some neurite outgrowth and Western blot experiments may be due to variations in the features of collected neurons and/or the distribution of GAL-1 at different spinal levels (McGraw et al., 2005a). It is impossible to gather the same profile of DRG neurons in every primary culture, and we cannot define what proportions of small/large neurons at which spinal level are predominantly obtained after the dissociation procedure.

The GDNF family of ligands (GFLs) includes GDNF, NRTN, ARTN and persephin (PSPN). These molecules are able to support the survival of dopaminergic midbrain neurons and facial and spinal motoneurons. In addition, GDNF, NRTN and ARTN, but not PSPN, have been shown to promote survival and neurite outgrowth of peripheral neurons (Paveliv et al., 2004; Peterziel and Strelau, 2006). The findings that NRTN and ARTN exhibited the bioactivity nearly comparable to GDNF in this study implicate common signaling pathway(s) among these GFLs. The actions of GFLs are initiated by binding to specific glycosyl phosphatidylinositol (GPI)-anchored GFL receptor α subtypes (GFRα); GDNF mainly binds to GFRα1, NRTN to GFRα2, and ARTN to GFRα3. The GFL-GFRα complex recruits transmembrane receptor tyrosine kinase RET to lipid rafts, resulting in the phosphorylation of tyrosine residues and activation of various intracellular signaling pathways (Airaksinen and Saarma, 2002). Although all GFLs basically act on RET-positive neurons, differential distribution of GFR receptors among the neurons (Josephson et al., 2001; Kashiba et al., 2003) may cause differential bioactivities among the GFLs. The less potent activity of NRTN and ARTN on the neurite length than GDNF is consistent with those on GAL-1 expression, and suggests that the subpopulation of NRTN- and ARTN-responsive neurons are slightly different from that of GDNF-responsive neurons. We observed that the GDNF-induced neurite outgrowth and upregulation of GAL-1 was attenuated by co-treatment with the anti-RET antibody, the PI3 K inhibitor LY294002, but not by the MEK inhibitor U0126. Therefore, the activation of RET-PI3K pathway in DRG neurons appears to be crucial for these GDNF actions on DRG neurons.

Since GAL-1 has been shown to promote axonal regeneration after injury (Horie et al., 1999; Sango et al., 2012a), the upregulation of GAL-1 concomitant with the promotion of neurite outgrowth implies the involvement of this molecule in the neurite outgrowth activity of GDNF. Contrary to our expectations, however, we failed to see significant differences between GAL-1 knockout and wild type mice in neurite outgrowth in the presence or absence of GDNF (Fig. 5). This finding suggests that other molecules can compensate for the lack of GAL-1 in the GDNF-induced neurite outgrowth. Some studies imply functional redundancies between GAL-1 and other lectin molecules, such as GAL-3 (Wang et al., 2006) and GAL-8 (Tsai et al., 2011). Our immunohistochemical analysis revealed predominant expression of GAL-3 in small IB4-binding DRG neurons with a considerable colocalization with GAL-1 (Fig. 6A). In addition, Western blot analysis showed GDNF-induced upregulation of GAL-3 in DRG cultures (Fig. 6B). These findings suggest that both GAL-1 and GAL-3 are downstream target molecules for the GDNF signaling in DRG neurons. Furthermore, recombinant GAL-3 used as a coating substratum exhibited slight but significant neurite outgrowth-promoting activities on cultured DRG neurons, whereas recombinant GAL-1 failed to show the activities (Fig. 6C). Therefore, it seems plausible that GAL-3 plays a more significant role than GAL-1 in GDNF-induced neurite outgrowth. There is room for further investigation on this possibility, and we plan to study the neurite outgrowth activity of GDNF under the state of selective knock down of GAL-3 and double knock down of GAL-1 and GAL-3.

According to the studies employing sciatic nerve injury models and DRG explant culture (Horie et al., 2004; Gaudet et al., 2009), some of the GAL-1 molecule released from neurons and Schwann cells can be converted to the oxidized form, which could promote axonal regeneration and Schwann cell migration via activating macrophages. However, this is not the case in the dissociated cell culture system of DRG, which contains very few macrophages. In fact, recombinant oxidized GAL-1 failed to promote neurite outgrowth from cultured adult rat DRG neurons (Inagaki et al.,

2000). In addition, recombinant GAL-1 used as a coating substratum failed to enhance neurite outgrowth (Fig. 6C). These findings suggests that GAL-1 upregulated by GDNF-RET-PI3K pathway further activates downstream signaling cascades inside the neurons, rather than it secretes to extracellular milieu and directly stimulates neurite outgrowth as an autocrine manner.

In summary, the results in the present study suggest that GAL-1 is a downstream target molecule of GDNF in adult rat DRG neurons. Since a growing body of evidence indicates that GDNF regulates the sensitivity of thermal nociceptors (Malin et al., 2006), GAL-1 may play a major role in mediating their actions, but the findings from GAL-1 knockout mice imply functional redundancy between GAL-1 and other molecules (*e.g.* GAL-3).

Acknowledgements

This study was supported by a Grant-in-aid for Scientific Research, from the Ministry of Education, Science, Sports and Culture, Japan (grant number: 22500324). This study was partly performed in the Cooperative Research Project Program of the Medical Institute of Bioregulation, Kyushu University. We thank Drs. Hitoshi Kawano, Nobuaki Maeda and Yukari Komuta for helpful suggestions, and Dr. Masami Tsukamoto, Junko Kimura-Kuroda, Hiroko Ueda, and the late Kyoko Ajiki for technical assistance.

References

Airaksinen, M.S., Saarma, M., 2002. The GDNF family: signalling, biological functions and therapeutic value. Nat. Rev. Neurosci. 3, 383–394.

Akazawa, C., Nakamura, Y., Sango, K., Horie, H., Kohsaka, S., 2004. Distribution of the galectin-1 mRNA in the rat nervous system: its transient upregulation in rat facial motor neurons after facial nerve axotomy. Neuroscience 125, 171–178.

Bennett, D.L., Michael, G.J., Ramachandran, N., Munson, J.B., Averill, S., Yan, Q., McMahon, S.B., Priestley, J.V., 1998. A distinct subgroup of small DRG cells express GDNF receptor components and GDNF is protective for these neurons after nerve injury. J. Neurosci. 18, 3059–3072.

Byrnes, K.R., Garay, J., Di Giovanni, S., De Biase, A., Knoblach, S.M., Hoffman, E.P., Movsesyan, V., Faden, A.I., 2006. Expression of two temporally distinct microglia-related gene clusters after spinal cord injury. Glia 53, 420–433.

Camby, I., Le Mercier, M., Lefranc, F., Kiss, R., 2006. Galectin-1: a small protein with major functions. Glycobiology 16, 137R–157R.

Fukaya, K., Hasegawa, M., Kadoya, T., Horie, H., Fujisawa, H., Hayashi, Y., Tachibana, O., Kida, S., Yamashita, J., 2003. Oxidized galectin-1 stimulates the migration of Schwann cells from both proximal and distal stumps of transected nerves and promotes axonal regeneration after peripheral nerve injury. J. Neuropathol. Exp. Neurol. 62, 162–172.

Gaudet, A.D., Leung, M., Poirier, F., Kadoya, T., Horie, H., Ramer, M.S., 2009. A role for galectin-1 in the immune response to peripheral nerve injury. Exp. Neurol. 220, 320–327.

Gavazzi, I., Kumar, R.D., McMahon, S.B., Cohen, J., 1999. Growth responses of different subpopulations of adult sensory neurons to neurotrophic factors in vitro. Eur. J. Neurosci. 11, 3405–3414.

Goldenberg, S.S., De Boni, U., 1983. Pure population of viable neurons from rabbit dorsal root ganglia, using gradients of Percoll. J. Neurobiol. 14, 195–206.

Horie, H., Inagaki, Y., Sohma, Y., Nozawa, R., Okawa, K., Hasegawa, M., Muramatsu, N., Kawano, H., Horie, M., Koyama, H., Sakai, I., Takeshita, K., Kowada, Y., Takano, M., Kadoya, T., 1999. Galectin-1 regulates initial axonal growth in peripheral nerves after axotomy. J. Neurosci. 19, 9964–9974.

Horie, H., Kadoya, T., Hikawa, N., Sango, K., Inoue, H., Takeshita, K., Asawa, R., Hiroi, T., Sato, M., Yoshioka, T., Ishikawa, Y., 2004. Oxidized galectin-1 stimulates macrophages to promote axonal regeneration in peripheral nerves after axotomy. J. Neurosci. 24, 1873–1880.

Hynes, M.A., Gitt, M., Barondes, S.H., Jessell, T.M., Buck, L.B., 1990. Selective expression of an endogenous lactose-binding lectin gene in subsets of central and peripheral neurons. J. Neurosci. 10, 1004–1013.

Imbe, H., Okamoto, K., Kadoya, T., Horie, H., Senba, E., 2003. Galectin-1 is involved in the potentiation of neuropathic pain in the dorsal horn. Brain Res. 993, 72–83.

Inagaki, Y., Sohma, Y., Horie, H., Nozawa, R., Kadoya, T., 2000. Oxidized galectin-1 promotes axonal regeneration in peripheral nerves but does not possess lectin properties. Eur. J. Biochem. 267, 2955–2964.

Ishibashi, S., Kuroiwa, T., Sakaguchi, M., Sun, L., Kadoya, T., Okano, H., Mizusawa, H., 2007. Galectin-1 regulates neurogenesis in the subventricular zone and promotes functional recovery after stroke. Exp. Neurol. 207, 302–313.

Iwamoto, M., Taguchi, C., Sasaguri, K., Kubo, K.Y., Horie, H., Yamamoto, T., Onozuka, M., Sato, S., Kadoya, T., 2010. The galectin-1 level in serum as a novel marker for stress. Glycoconj. J. 27, 419–425.

Iwase, T., Jung, C.G., Bae, H., Zhang, M., Soliven, B., 2005. Glial cell line-derived neurotrophic factor-induced signaling in Schwann cells. J. Neurochem. 94, 1488–1499.

Josephson, A., Widenfalk, J., Trifunovski, A., Widmer, H.R., Olson, L., Spenger, C., 2001. GDNF and NGF family members and receptors in human fetal and adult spinal cord and dorsal root ganglia. J. Comp. Neurol. 440, 204–217.

Kajitani, K., Nomaru, H., Ifuku, M., Yutsudo, N., Dan, Y., Miura, T., Tsuchimoto, D., Sakumi, K., Kadoya, T., Horie, H., Poirier, F., Noda, M., Nakabeppu, Y., 2009. Galectin-1 promotes basal and kainate-induced proliferation of neural progenitors in the dentate gyrus of adult mouse hippocampus. Cell Death Differ. 216, 417–427.

Kashiba, H., Uchida, Y., Senba, E., 2003. Distribution and colocalization of NGF and GDNF family ligand receptor mRNAs in dorsal root and nodose ganglion neurons of adult rats. Brain Res. Mol. Brain Res. 110, 52–62.

Kato, T., Ren, C.H., Wada, M., Kawanami, T., 2005. Galectin-1 as a potential therapeutic agent for amyotrophic lateral sclerosis. Curr. Drug Targets 6, 407–418.

Kuklinski, S., Vladimirova, V., Waha, A., Kamata, H., Pesheva, P., Probstmeier, R., 2003. Expression of galectin-3 in neuronally differentiating PC12 cells is regulated both via Ras/MAPK-dependent and -independent signalling pathways. J. Neurochem. 87, 1112–1124.

Kurihara, D., Ueno, M., Tanaka, T., Yamashita, T., 2010. Expression of galectin-1 in immune cells and glial cells after spinal cord injury. Neurosci. Res. 66, 266–270.

Kurushima, H., Ohno, M., Miura, T., Nakamura, T.Y., Horie, H., Kadoya, T., Ooboshi, H., Kitazono, T., Ibayashi, S., Iida, M., Nakabeppu, Y., 2005. Selective induction of DeltaFosB in the brain after transient forebrain ischemia accompanied by an increased expression of galectin-1, and the implication of DeltaFosB and galectin-1 in neuroprotection and neurogenesis. Cell Death Differ. 12, 1078–1096.

Le Mercier, M., Fortin, S., Mathieu, V., Kiss, R., Lefranc, F., 2010. Galectins and gliomas. Brain Pathol. 20, 17–27.

Leclere, P., Ekström, P., Edström, A., Priestley, J., Averill, S., Tonge, D.A., 1998. Effects of glial cell line-derived neurotrophic factor on axonal growth and apoptosis in adult mammalian sensory neurons in vitro. Neuroscience 82, 545–558.

Lekishvili, T., Hesketh, S., Brazier, M.W., Brown, D.R., 2006. Mouse galectin-1 inhibits the toxicity of glutamate by modifying NR1 NMDA receptor expression. Eur. J. Neurosci. 24, 3017–3025.

Malin, S.A., Molliver, D.C., Koerber, H.R., Cornuet, P., Frye, R., Albers, K.M., Davis, B.M., 2006. Glial cell line-derived neurotrophic factor family members sensitize nociceptors in vitro and produce thermal hyperalgesia in vivo. J. Neurosci. 26, 8588–8599.

McGraw, J., McPhail, L.T., Oschipok, L.W., Horie, H., Poirier, F., Steeves, J.D., Ramer, M.S., Tetzlaff, W., 2004. Galectin-1 in regenerating motoneurons. Eur. J. Neurosci. 20, 2872–2880.

McGraw, J., Gaudet, A.D., Oschipok, L.W., Kadoya, T., Horie, H., Steeves, J.D., Tetzlaff, W., Ramer, M.S., 2005a. Regulation of neuronal and glial galectin-1 expression by peripheral and central axotomy of rat primary afferent neurons. Exp. Neurol. 195, 103–114.

McGraw, J., Gaudet, A.D., Oschipok, L.W., Steeves, J.D., Poirier, F., Tetzlaff, W., Ramer, M.S., 2005b. Altered primary afferent anatomy and reduced thermal sensitivity in mice lacking galectin-1. Pain 114, 7–18.

McMahon, S.B., Bennett, D.L.H., 2000. Glial cell line-derived neurotrophic factor and nociceptive neurons. In: Wood, J.N. (Ed.), Molecular Basis of Pain Modulation. Wiley-Liss, New York, pp. 65–86.

Molliver, D.C., Wright, D.E., Leitner, M.L., Parsadanian, A.S., Doster, K., Wen, D., Yan, Q., Snider, W.D., 1997. IB4-binding DRG neurons switch from NGF to GDNF dependence in early postnatal life. Neuron 19, 849–861.

North, A.J., Galazkiewicz, B., Byers, T.J., Glenney Jr, J.R., Small, J.V., 1993. Complementary distributions of vinculin and dystrophin define two distinct sarcolemma domains in smooth muscle. J. Cell Biol. 120, 1159–1167.

Paratcha, G., Ledda, F., Ibáñez, C.F., 2003. The neural cell adhesion molecule NCAM is an alternative signaling receptor for GDNF family ligands. Cell 113, 867–879.

Paveliv, M., Airaksinen, M.S., Saarma, M., 2004. GDNF family ligands activate multiple events during axonal growth in mature sensory neurons. Mol. Cell. Neurosci. 25, 453–459.

Peng, W., 2012. Intravenous immunoglobulin treatment on anti-GM1 antibodies associated neuropathies inhibits cholera toxin and galectin-1 binding to ganglioside GM1. Immunol. Lett. 143, 146–151.

Pesheva, P., Kuklinski, S., Biersack, H.J., Probstmeier, R., 2000. Nerve growth factor-mediated expression of galectin-3 in mouse dorsal root ganglion neurons. Neurosci. Lett. 293, 37–40.

Peterziel, H., Strelau, J., 2006. GDNF and related proteins. In: Lajtha, A. (Ed.), Handbook of Neurochemistry and Molecular Neurobiology. In: Lim, R. (Ed.), Neuroactive Proteins and Peptides, third ed. Springer+Business Media LLC, New York, pp. 69–91.

Plaza-Menacho, I., van der Sluis, T., Hollema, H., Gimm, O., Buys, C.H., Magee, A.I., Isacke, C.M., Hofstra, R.M., Eggen, B.J., 2007. Ras/ERK1/2-mediated STAT3 Ser727 phosphorylation by familial medullary thyroid carcinoma-associated RET mutants induces full activation of STAT3 and is required for c-fos promoter activation, cell mitogenicity, and transformation. J. Biol. Chem. 282, 6415–6424.

Puche, A.C., Poirier, F., Hair, M., Bartlett, P.F., Key, B., 1996. Role of galectin-1 in the developing mouse olfactory system. Dev. Biol. 179, 274–287.

Qu, W.S., Wang, Y.H., Ma, J.F., Tian, D.S., Zhang, Q., Pan, D.J., Yu, Z.Y., Xie, M.J., Wang, J.P., Wang, W., 2011. Galectin-1 attenuates astrogliosis-associated injuries and improves recovery of rats following focal cerebral ischemia. J. Neurochem. 116, 217–226.

Regan, L.J., Dodd, J., Barondes, S.H., Jessell, T.M., 1986. Selective expression of endogenous lactose-binding lectins and lactoseries glycoconjugates in subsets of rat sensory neurons. Proc. Natl. Acad. Sci. USA 83, 2248–2252.

Rossner, M., Yamada, K.M., 2004. What's in a picture? The temptation of image manipulation. J. Cell Biol. 166, 11–15.

Sakaguchi, M., Imaizumi, Y., Shingo, T., Tada, H., Hayama, K., Yamada, O., Morishita, T., Kadoya, T., Uchiyama, N., Shimazaki, T., Kuno, A., Poirier, F., Hirabayashi, J., Sawamoto, K., Okano, H., 2010. Regulation of adult neural progenitor cells by galectin-1/beta1 integrin interaction. J. Neurochem. 113, 1516–1524.

Sango, K., Oohira, A., Ajiki, K., Tokashiki, A., Horie, M., Kawano, H., 2003. Phosphacan and neurocan are repulsive substrata for adhesion and neurite extension of adult rat dorsal root ganglion neurons in vitro. Exp. Neurol. 182, 1–11.

Sango, K., Tokashiki, A., Ajiki, K., Horie, M., Kawano, H., Watabe, K., Horie, H., Kadoya, T., 2004. Synthesis, localization and externalization of galectin-1 in mature dorsal root ganglion neurons and Schwann cells. Eur. J. Neurosci. 19, 55–64.

Sango, K., Yanagisawa, H., Takaku, S., 2007. Expression and histochemical localization of ciliary neurotrophic factor in cultured adult rat dorsal root ganglion neurons. Histochem. Cell Biol. 128, 35–43.

Sango, K., Yanagisawa, H., Komuta, Y., Si, Y., Kawano, H., 2008. Neuroprotective properties of ciliary neurotrophic factor for cultured adult rat dorsal root ganglion neurons. Histochem. Cell Biol. 130, 669–679.

Sango, K., Yanagisawa, H., Kawakami, E., Takaku, S., Ajiki, K., Watabe, K., 2011. Spontaneously immortalized Schwann cells from adult Fischer rat as a valuable tool for exploring neuron-Schwann cell interactions. J. Neurosci. Res. 89, 898–908.

Sango, K., Yanagisawa, H., Watabe, K., Horie, H., Kadoya, T., 2012a. Chapter 3: Galectin-1 as a multifunctional molecule in the peripheral nervous system after injury. In: Rayegani, S.M. (Ed.), Basic Principles of Peripheral Nerve Disorders. InTech d.o.o, Rijeka, Croatia, pp. 31–46, <http://www.intechopen.com/books/basic-principles-of-peripheral-nerve-disorders/galectin-1-as-a-multifunctional-molecule-in-the-peripheral-nervous-system-after-injury>.

Sango, K., Kawakami, E., Yanagisawa, H., Takaku, S., Tsukamoto, M., Utsunomiya, K., Watabe, K., 2012b. Myelination in coculture of established neuronal and Schwann cell lines. Histochem. Cell Biol. 137, 829–839.

Stancic, M., van Horssen, J., Thijssen, V.L., Gabius, H.J., van der Valk, P., Hoekstra, D., Baron, W., 2011. Increased expression of distinct galectins in multiple sclerosis lesions. Neuropathol. Appl. Neurobiol. 37, 654–671.

Starossom, S.C., Mascanfroni, I.D., Imitola, J., Cao, L., Raddassi, K., Hernandez, S.F., Bassil, R., Croci, D.O., Cerliani, J.P., Delacour, D., Wang, Y., Elyaman, W., Khoury, S.J., Rabinovich, G.A., 2012. Galectin-1 deactivates classically activated microglia and protects from inflammation-induced neurodegeneration. Immunity 37, 249–263.

Tarsa, L., Goda, Y., 2002. Synaptophysin regulates activity-dependent synapse formation in cultured hippocampal neurons. Proc. Natl. Acad. Sci. USA 99, 1012–1016.

Tsai, C.M., Guan, C.H., Hsieh, H.W., Hsu, T.L., Tu, Z., Wu, K.J., Lin, C.H., Lin, K.I., 2011. Galectin-1 and galectin-8 have redundant roles in promoting plasma cell formation. J. Immunol. 187, 1643–1652.

Vent, J., Wyatt, T.A., Smith, D.D., Banerjee, A., Ludueña, R.F., Sisson, J.H., Hallworth, R., 2005. Direct involvement of the isotype-specific C-terminus of beta tubulin in ciliary beating. J. Cell Sci. 118, 4333–4341.

Wang, W., Park, J.W., Wang, J.L., Patterson, R.J., 2006. Immunoprecipitation of spliceosomal RNAs by antisera to galectin-1 and galectin-3. Nucleic Acids Res. 34, 5166–5174.

Watabe, K., Fukuda, T., Tanaka, J., Honda, H., Toyohara, K., Sakai, O., 1995. Spontaneously immortalized adult mouse Schwann cells secrete autocrine and paracrine growth-promoting activities. J. Neurosci. Res. 41, 279–290.

Wu, Z.Z., Pan, H.L., 2004. Tetrodotoxin-sensitive and -resistant Na+ channel currents in subsets of small sensory neurons of rats. Brain Res. 1029, 251–258.

Yamane, J., Nakamura, M., Iwanami, A., Sakaguchi, M., Katoh, H., Yamada, M., Momoshima, S., Miyao, S., Ishii, K., Tamaoki, N., Nomura, T., Okano, H.J., Kanemura, Y., Toyama, Y., Okano, H., 2010. Transplantation of galectin-1-expressing human neural stem cells into the injured spinal cord of adult common marmosets. J. Neurosci. Res. 88, 1394–1405.

Zhang, L., Chang, M., Li, H., Hou, S., Zhang, Y., Hu, Y., Han, W., Hu, L., 2007. Proteomic changes of PC12 cells treated with proteasomal inhibitor PSI. Brain Res. 1153, 196–203.

Research article

8-Oxoguanine causes neurodegeneration during MUTYH-mediated DNA base excision repair

Zijing Sheng,[1,2] Sugako Oka,[1,2] Daisuke Tsuchimoto,[1,2] Nona Abolhassani,[1] Hiroko Nomaru,[1] Kunihiko Sakumi,[1,2] Hidetaka Yamada,[1,3] and Yusaku Nakabeppu[1,2]

[1]Division of Neurofunctional Genomics, Department of Immunobiology and Neuroscience, Medical Institute of Bioregulation, and [2]Research Center for Nucleotide Pool, Kyushu University, Fukuoka, Japan. [3]Cognitive and Molecular Research Institute of Brain Diseases, Kurume University School of Medicine, Kurume, Japan.

8-Oxoguanine (8-oxoG), a common DNA lesion caused by reactive oxygen species, is associated with carcinogenesis and neurodegeneration. Although the mechanism by which 8-oxoG causes carcinogenesis is well understood, the mechanism by which it causes neurodegeneration is unknown. Here, we report that neurodegeneration is triggered by MUTYH-mediated excision repair of 8-oxoG–paired adenine. Mutant mice lacking 8-oxo-2′-deoxyguanosine triphosphate–depleting (8-oxo-dGTP–depleting) MTH1 and/or 8-oxoG–excising OGG1 exhibited severe striatal neurodegeneration, whereas mutant mice lacking MUTYH or OGG1/MUTYH were resistant to neurodegeneration under conditions of oxidative stress. These results indicate that OGG1 and MTH1 are protective, while MUTYH promotes neurodegeneration. We observed that 8-oxoG accumulated in the mitochondrial DNA of neurons and caused calpain-dependent neuronal loss, while delayed nuclear accumulation of 8-oxoG in microglia resulted in PARP-dependent activation of apoptosis-inducing factor and exacerbated microgliosis. These results revealed that neurodegeneration is a complex process caused by 8-oxoG accumulation in the genomes of neurons and microglia. Different signaling pathways were triggered by the accumulation of single-strand breaks in each type of DNA generated during base excision repair initiated by MUTYH, suggesting that suppression of MUTYH may protect the brain under conditions of oxidative stress.

Introduction

The DNA and precursor nucleotides in living organisms are always in danger of oxidation by ROS that are inevitably generated as a by-product of oxygen respiration and are products of host defense and signal transduction mechanisms (1, 2). If oxidized lesions accumulate in DNA, mutagenesis or cell death may result (3–5). Among all nucleobases, guanine is known to be the most susceptible to oxidation, and its simple oxidized form, 8-oxoguanine (8-oxoG), which can pair with adenine as well as cytosine, is one of the major oxidation products in DNA and nucleotides (6, 7).

Mammalian cells are equipped with elaborate means of minimizing accumulation of 8-oxoG in DNA. 8-oxo-2′-deoxyguanosine triphosphatase (8-oxo-dGTPase) encoded by *MTH1* hydrolyzes 8-oxo-dGTP to 8-oxo-dGMP and pyrophosphate in nucleotide pools, thereby avoiding incorporation of 8-oxo-dGMP into DNA (8, 9). 8-OxoG DNA glycosylase 1 encoded by *OGG1* excises 8-oxoG paired with cytosine in DNA (10), while adenine DNA glycosylase encoded by *MUTYH* removes the adenine inserted opposite 8-oxoG in template DNA during DNA replication (11), thus preventing mutagenesis. Mutant mice lacking these genes exhibit increased spontaneous mutation rate and susceptibility to carcinogenesis with increased accumulation of 8-oxoG in DNA (12–15).

Oxidative stress is considered to be important in the etiology of several neurodegenerative disorders, and it has been shown that 8-oxoG levels are significantly increased in mitochondrial DNA (mtDNA) as well as nuclear DNA (nDNA) in the brains of patients with Parkinson's disease (PD) (16), Alzheimer's disease (AD) (17), and Huntington's disease (HD) (18) in comparison with control brains. Expression levels of MTH1, OGG1, and MUTYH are also significantly altered in the brains of such patients (16, 19–22), suggesting that their altered expression along with accumulation of 8-oxoG in brain cause neurodegeneration; however, how 8-oxoG and these enzymes are associated with the neurodegenerative process is poorly understood.

The striatum plays a key role in motor, cognitive, and motivational processes (23). Abnormal striatal function is involved in several neurodegenerative disorders, such as PD, AD, and HD. The inhibitor of mitochondrial succinate dehydrogenase 3-nitropropionic acid (3-NP), a naturally occurring plant toxin, has been shown to cause striatal degeneration and motor impairments in animals similar to those seen in HD (24, 25). It has been established that administration of 3-NP to rodents and nonhuman primates replicates most of the clinical and pathophysiological hallmarks of HD, including spontaneous choreiform and dystonic movements, frontal-type cognitive deficits, and progressive heterogeneous striatal degeneration, at least partially by apoptosis (26). We have shown that increased expression of human MTH1 in mouse striatum efficiently suppresses such striatal degeneration, accompanied by effective suppression of the 8-oxoG accumulation in the striatum induced by 3-NP (27). However, it is not clear to what extent 8-oxoG accumulated in DNA is responsible for the neurodegeneration, because MTH1 can hydrolyze oxidized forms of ATP, GTP, and dATP as well as dGTP (28). Moreover, it is not known which type of DNA (nDNA and/or mtDNA) harboring 8-oxoG is associated with such neurodegeneration, nor is it known how the neuronal loss occurs.

Conflict of interest: The authors have declared that no conflict of interest exists.

Citation for this article: *J Clin Invest.* 2012;122(12):4344–4361. doi:10.1172/JCI65053.

In the present study, we investigated the mechanism by which 8-oxoG is involved in neurodegeneration using mutant mice lacking *Ogg1*, *Mth1*, and/or *Mutyh* genes under conditions of oxidative stress. We demonstrated that OGG1 cooperatively protects brain with MTH1, reflecting a beneficial role of DNA repair and, intriguingly, that DNA repair by MUTYH is required for neurodegeneration upon 8-oxoG accumulation in brain, thus exhibiting a harmful role of DNA repair.

Results

Mth1/Ogg1-double-KO mice are highly vulnerable to striatal degeneration caused by chronic exposure to 3-NP. We first immunohistochemically confirmed the expression of MTH1 and OGG1 proteins in mouse striatum. Specific immunoreactivities (IRs) for both MTH1 and OGG1 were detected only in WT striatum, but not in *Mth1-KO* or *Ogg1-KO* striatum, respectively (Supplemental Figure 1; supplemental material available online with this article; doi:10.1172/JCI65053DS1). Immunofluorescence microscopy revealed that cytoplasmic IRs for MTH1 and OGG1 were predominantly detected in DARPP32-positive medium spiny neurons (MSNs) in WT striatum (Figure 1A). Immunoelectron microscopy confirmed that MTH1 and OGG1 IRs were distributed in the cytoplasm and nucleus only in the WT striatum (Supplemental Figure 2). It is evident that the OGG1 cytoplasmic IR colocalized with mitochondrial HSP60 IR (Figure 1A). Thus, we hypothesized that MTH1 and OGG1 play important roles in protecting MSNs in the striatum from oxidative stress.

To evaluate this hypothesis, we examined the effects of 3-NP on motor function in WT and mutant mouse strains lacking *Ogg1* and/or *Mth1* genes, in small cohorts (Supplemental Figure 3). Chronic exposure of mice to 3-NP resulted in motor impairments. Individual pairwise comparisons to WT mice revealed that *Mth1/Ogg1*-double-KO (*Mth1/Ogg1*-DKO) and to a lesser extent *Ogg1*-KO mice exhibited a statistically significant decline of travel distance in an open-field test, but no significant difference was found between *Mth1*-KO and WT mice ($P < 0.05$, $P < 0.02$, respectively). We then examined the effects of 3-NP on WT and *Mth1/Ogg1*-DKO mice in large cohorts. First, we evaluated the 3-NP–induced motor symptoms in WT and *Mth1/Ogg1*-DKO mice based on neurological scores (refs. 29, 30, and Supplemental Figure 4) and found that *Mth1/Ogg1*-DKO mice exhibited more severe motor symptoms. A quantitative analysis of spontaneous locomotor behavior in their home cages during day and night revealed that *Mth1/Ogg1*-DKO mice show more hypolocomotor activity in the home cages during the night on the fifth and sixth days of 3-NP exposure (Supplemental Figure 5). An open-field test showed that the distance travelled by DKO mice in the open field was significantly reduced, to 52% of the level seen in WT mice after exposure to 3-NP for 7 days, and vertical rearing was also significantly reduced in DKO mice to 59% of the level seen in WT mice (Figure 1B and Supplemental Videos 1 and 2). *Mth1/Ogg1*-DKO and WT mice both exhibited modest reductions in performance on a rotarod test after exposure to 3-NP for 7 days; however, there was no significant difference between the 2 groups of mice (data not shown), indicating that the significantly decreased motor activity in *Mth1/Ogg1-DKO* mice was not due to increased muscle disorder.

More severe striatal degeneration was observed in DKO mice than in WT mice after 7 days of exposure to 3-NP (Figure 1C). Laser scanning confocal immunofluorescence microscopy (LSCIM) revealed that most DARPP32-positive MSNs were lost and increased numbers of F4/80-positive microglia were detected in the DKO striatum, especially in the dorsolateral part of the striatum, after exposure to 3-NP for 7 days (Figure 1D), indicating that the 3-NP induces striatal degeneration accompanied by microgliosis. Thus, we concluded that the double deficiency in MTH1 and OGG1 renders the striatum highly vulnerable to 3-NP–induced neurodegeneration.

Significant increase in the level of mitochondrial 8-oxoG, but not nuclear 8-oxoG, in the Mth1/Ogg1-DKO striatum after exposure to 3-NP. We previously established that 8-oxoG in mtDNA can be visualized in tissue sections treated only with RNase before incubation with anti–8-oxo-dG, while 8-oxoG in nDNA can be detected in sections treated with RNase and HCl before incubation with the antibody (31, 32). Most neurons in the DKO striatum were lost after exposure to 3-NP for 7 days (Figure 1, C and D); therefore, it is likely that 8-oxoG in nDNA may not be detected in the striatum after 7 days of exposure to 3-NP. We found that MSNs expressing DARPP32 were still detectable in the striata of WT and DKO mice after exposure to 3-NP for 4 days (Figure 2A); therefore, we examined nuclear 8-oxoG levels by LC-MS/MS analysis of striatal nDNA prepared after exposure to 3-NP for 1 or 3 days using stable isotope-labeled [^{15}N5] 8-oxo-dG as an internal standard. Nuclear 8-oxo-dG levels were not significantly increased in either group after exposure to 3-NP, although DKO mice had higher basal levels of nuclear 8-oxo-dG in the striatum than did WT mice (Figure 2B). LSCIM following pretreatment of sections with HCl revealed that exposure to 3-NP for 4 days causes a marginal increase in nuclear 8-oxoG IR in the DKO striatum in agreement with the results of LC-MS/MS analysis (data not shown). These results indicate that 8-oxoG is not highly accumulated in nDNA prior to loss of MSNs in the striatum.

Exposure to 3-NP for 7 days caused significant increases in cytoplasmic 8-oxoG IR in the *Mth1/Ogg1*-DKO striatum in comparison with WT or untreated samples without HCl pretreatment, suggesting 8-oxoG accumulation in mtDNA (Figure 3, A and B). LSCIM revealed that DARPP32-positive MSNs in the DKO striatum exhibited strong cytoplasmic 8-oxoG IR without HCl pretreatment after exposure to 3-NP for 4 days (Figure 3C) and that this IR was colocalized with that for mitochondrial transcription factor A (TFAM) with which mtDNA is packaged (ref. 33 and Figure 3D), indicating that 8-oxoG accumulates mostly in the mtDNA of MSNs in the DKO striatum. The basal level of mitochondrial 8-oxoG in DKO MSNs was 8-fold higher than that in WT MSNs without exposure to 3-NP, indicating an increased spontaneous accumulation of 8-oxoG in the mtDNA. After 4 days of 3-NP exposure, the levels were significantly increased in both WT and DKO MSNs; the level in DKO MSNs was 3.5 times higher than that in WT MSNs (Figure 3, E and F).

On the seventh day of exposure to 3-NP, we observed significantly increased IR for single-stranded DNA (ssDNA) in the cytoplasm of neurons in the DKO striatum, in agreement with selective damage such as single-strand breaks (SSBs) in their mtDNA. Cells with small nuclei exhibited nuclear ssDNA IRs (Figure 3G), indicating that the nuclei of microglia also accumulate DNA damage. On the seventh day of exposure to 3-NP, we noticed that microglia proliferating in the region of striatum, where MSNs were largely lost, exhibit nuclear, and to a lesser extent cytoplasmic, 8-oxoG IR (Figure 3H).

Independent activation of calpain and apoptosis-inducing factor during the striatal degeneration caused by 3-NP. We previously showed that *Ogg1*-KO cells expressing a nuclear form of human OGG1 accumulate 8-oxoG selectively in mtDNA under oxidative stress and

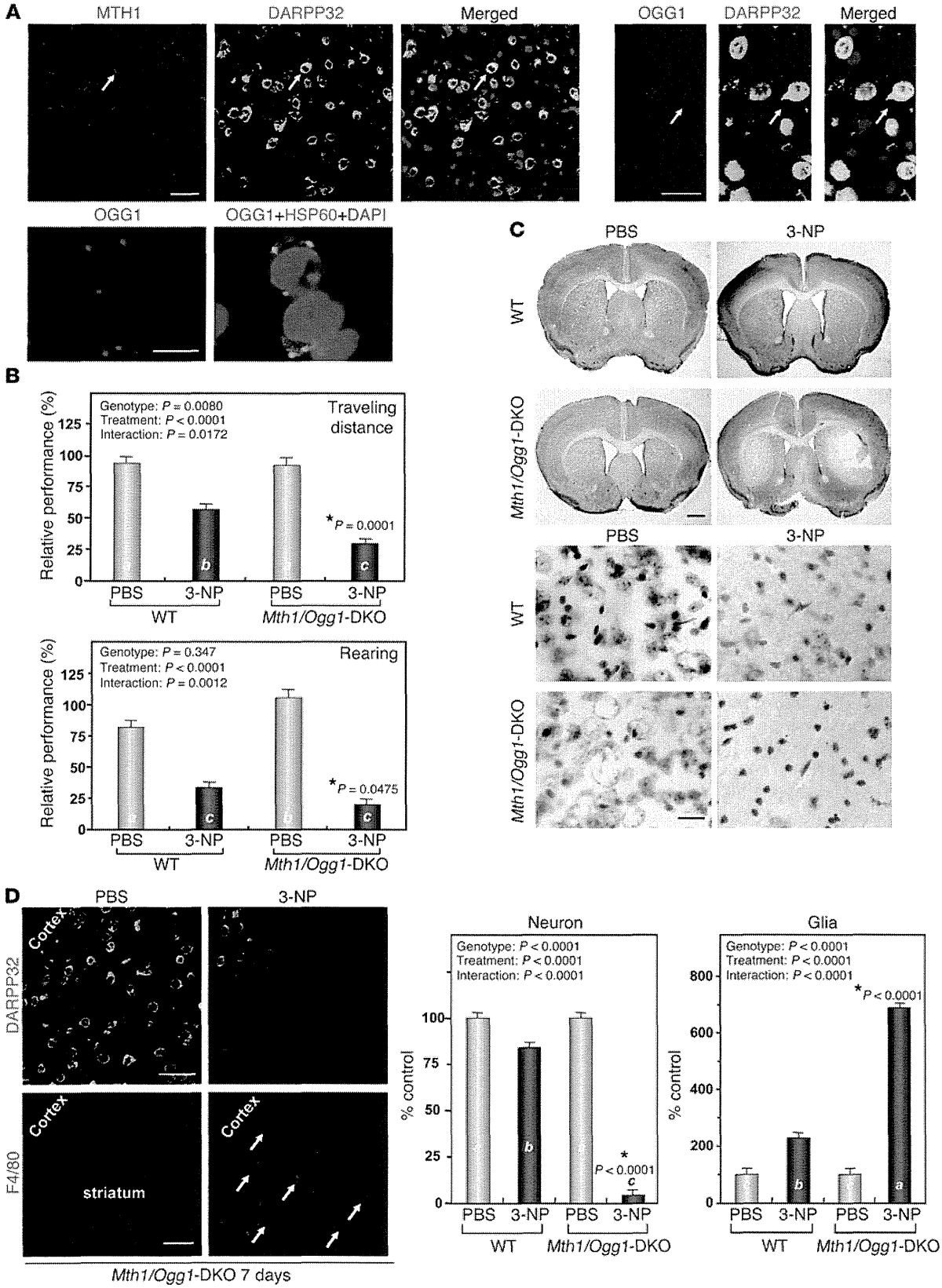
A
MTH1
DARPP32
Merged
OGG1
DARPP32
Merged
OGG1
OGG1+HSP60+DAPI
B
Genotype: P = 0.0080
Treatment: P < 0.0001
Interaction: P = 0.0172
Traveling distance
Relative performance (%)
*P = 0.0001
PBS
3-NP
PBS
3-NP
WT
Mth1/Ogg1-DKO
Genotype: P = 0.347
Treatment: P < 0.0001
Interaction: P = 0.0012
Rearing
*P = 0.0475
C
PBS
3-NP
WT
Mth1/Ogg1-DKO
D
PBS
3-NP
DARPP32
F4/80
Cortex
striatum
Mth1/Ogg1-DKO 7 days
Neuron
Genotype: P < 0.0001
Treatment: P < 0.0001
Interaction: P < 0.0001
% control
*P < 0.0001
Glia
Genotype: P < 0.0001
Treatment: P < 0.0001
Interaction: P < 0.0001
*P < 0.0001

Figure 1
Mth1/Ogg1-DKO mice are extremely vulnerable to 3-NP–induced motor impairments and striatal degeneration. (**A**) MTH1 (upper left panels) and OGG1 (upper right panels) IRs (red) were abundant in WT striatum and were predominantly localized in DARPP32-positive neurons (green). Arrows show positively stained neurons. Scale bar: 20 μm. OGG1 IR (red) in the cytoplasm colocalized with HSP60 IR (green) (lower panels). Scale bar: 10 μm. (**B**) Motor impairments after exposure to 3-NP. Numbers of animals examined per condition are 14 (WT, PBS), 21 (WT, 3-NP), 11 (*Mth1/Ogg1*-DKO, PBS), and 22 (*Mth1/Ogg1*-DKO, 3-NP). (**C**) Striatal degeneration as revealed by Nissl staining. Upper panels, lower magnification; scale bar: 1 mm. Lower panels: higher magnification, scale bar: 20 μm. (**D**) Loss of MSNs expressing DARPP32 (green) and microgliosis as detected by F4/80 (red) staining. Arrows indicate F4/80-positive microglia. The numbers of neurons and glia in the dorsolateral striatum were counted on Nissl-stained sections, $n = 3$ for each group. Scale bars: 20 μm (upper); 100 μm (lower). In **B** and **D**, data in each bar graph are shown with LS means ± SEM, and *P* values for the effects of genotype, treatment, and interaction between genotype, and treatment are shown. Levels not connected with the same letter are significantly different (Tukey's HSD test). **P*, compared with WT mice exposed to 3-NP.

demonstrated that the accumulation of 8-oxoG in mtDNA causes mitochondrial dysfunction and Ca^{2+} release, thereby activating calpain to execute caspase-independent cell death (34). Because 8-oxoG was selectively accumulated in the mtDNA of MSNs in *Mth1/Ogg1*-DKO striatum after 3-NP exposure (Figure 3, A–F), we examined whether accumulation of 8-oxoG in mtDNA in the striatum activates calpain. Western blotting analysis of α-spectrin, a substrate for calpain (35), revealed that 3-NP exposure for 4 or 7 days caused markedly increased processing of α-spectrin in the *Mth1/Ogg1*-DKO striatum in comparison with WT (Figure 4A). The relative level of a 145-kDa band corresponding to a major calpain-cleaved product (35) was significantly increased in the DKO striatum after exposure to 3-NP, while such increased cleavage of α-spectrin was barely seen in WT striatum (Figure 4A). It is likely that the dose of 3-NP (120 mg/kg/d) is not enough to activate calpain in WT striatum, thereby causing little neurodegeneration (Figure 1), consistent with a previous suggestion that the activation of calpain observed in 3-NP–treated animals is probably instrumental in striatal degeneration (36). In PBS-treated striatum, α-spectrin IR was detected in the nuclei of neurons in both WT and DKO striatum; however, we noticed that perinuclear IR for α-spectrin was evident in the DKO striatum after exposure to 3-NP for 4 days (Figure 4B), indicating that the calpain-dependent processing of α-spectrin results in its altered intracellular localization (37). Because such perinuclear IR of α-spectrin was exclusively detected in DARPP32-positive neurons in the DKO striatum after exposure to 3-NP, calpain must be selectively activated in MSNs (Figure 4C).

Using *Ogg1*-KO cells, which express a mitochondrial form of human OGG1, we previously demonstrated that the selective accumulation of 8-oxoG in nDNA causes PARP-dependent nuclear translocation of apoptosis-inducing factor (AIF) and that the cells subsequently underwent PARP/AIF-dependent cell death (34). We therefore examined whether PARP and AIF are involved in 3-NP–induced striatal degeneration. LSCIM with anti-poly(ADP-ribose) (anti-PAR) or anti-AIF antibodies revealed a significant accumulation of PAR-polymer and AIF in the striatal region of DKO mice from which MSNs were largely lost after exposure to 3-NP for 7 days (Figure 4D). We observed increased numbers of F4/80-positive microglia in this region (Figure 1D), and IRs for PAR and AIF were mostly detected in the nuclei of microglia (Figure 5A). No AIF or PAR IR was seen in MSNs (Figure 5B), and no AIF IR was seen in GFAP-positive astrocytes after exposure to 3-NP (Figure 5C). Western blotting analysis of AIF revealed that exposure to 3-NP for 7 days caused significant accumulation of a 57-kDa form of AIF, a processed nuclear form of AIF (38), only in the DKO striatum, but not in the WT striatum (Figure 5D), indicating that delayed activation of AIF accompanied by PAR-polymer accumulation occurs selectively in microglia in the DKO striatum exposed to 3-NP. These data indicate that activation of calpain is restricted to MSNs and that activation of AIF is restricted to microglia.

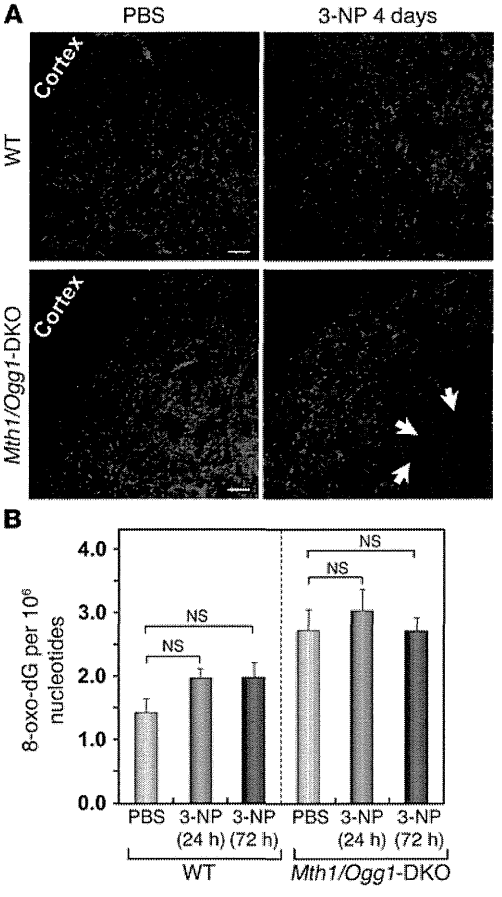

Figure 2
Nuclear 8-oxo–dG levels in striatum detected by LC-MS/MS analysis. (**A**) DARPP32-positive MSNs were still detected on the fourth day of 3-NP exposure. Arrows show that DARPP32 staining was slightly decreased in the *Mth1/Ogg1*-DKO striatum compared with WT striatum exposed to 3-NP. Scale bar: 50 μm. (**B**) Nuclear 8-oxo–dG levels in striatum measured by LC-MS/MS analysis. The number of animals examined is 5 for each group. Residues of 8-oxo–dG per 10^6 nucleotides in nuclear DNA determined by LC-MS/MS are shown as LS means ± SEM. Nuclear 8-oxo–dG levels were not significantly increased in either group after exposure to 3-NP (Student's *t* test).

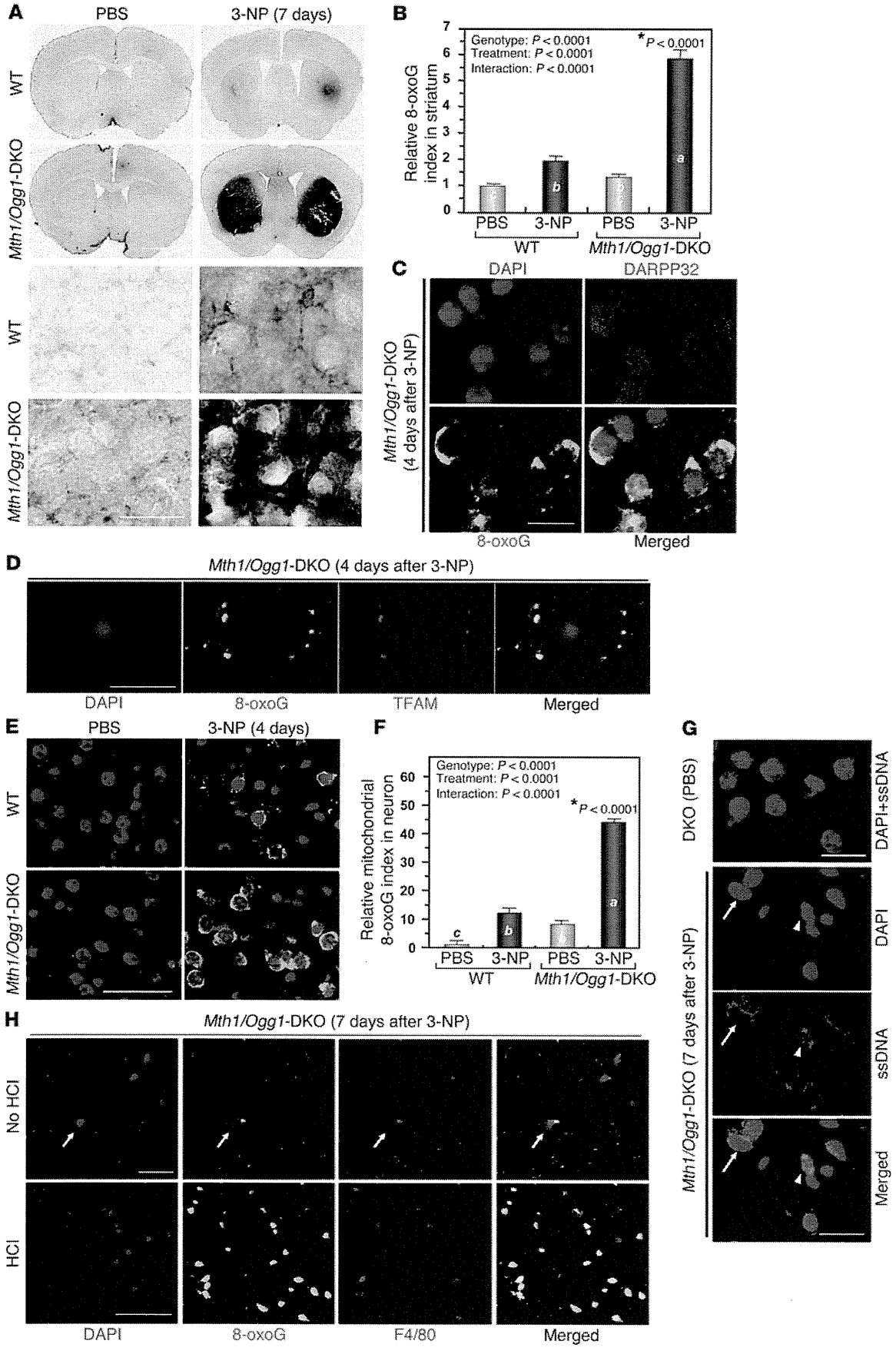
A
PBS
3-NP (7 days)
WT
Mth1/Ogg1-DKO
WT
Mth1/Ogg1-DKO
B
Relative 8-oxoG index in striatum
Genotype: P < 0.0001
Treatment: P < 0.0001
Interaction: P < 0.0001
*P < 0.0001
PBS
3-NP
PBS
3-NP
WT
Mth1/Ogg1-DKO
C
DAPI
DARPP32
Mth1/Ogg1-DKO (4 days after 3-NP)
8-oxoG
Merged
D
Mth1/Ogg1-DKO (4 days after 3-NP)
DAPI
8-oxoG
TFAM
Merged
E
PBS
3-NP (4 days)
WT
Mth1/Ogg1-DKO
F
Relative mitochondrial 8-oxoG index in neuron
Genotype: P < 0.0001
Treatment: P < 0.0001
Interaction: P < 0.0001
*P < 0.0001
PBS
3-NP
PBS
3-NP
WT
Mth1/Ogg1-DKO
G
DKO (PBS)
Mth1/Ogg1-DKO (7 days after 3-NP)
DAPI+ssDNA
DAPI
ssDNA
Merged
H
Mth1/Ogg1-DKO (7 days after 3-NP)
No HCl
HCl
DAPI
8-oxoG
F4/80
Merged

Figure 3
Mth1/Ogg1-DKO striatum exhibits significantly increased accumulation of 8-oxoG in MSNs and microglia after exposure to 3-NP. (**A**) DKO mice exhibited stronger cytoplasmic 8-oxoG IR in the striatum compared with WT mice. Sections were pretreated only with RNase. Upper panels: lower magnification, scale bar: 2 mm. Lower panels: higher magnification. Images were obtained using differential interference contrast (DIC) microscopy, scale bar: 20 μm. (**B**) Quantitative measurement of 8-oxoG IR in the striatum shown in **A** (n = 8 for each group). (**C**) Cytoplasmic 8-oxoG IR was detected in DARPP32-positive neurons. Scale bar: 20 μm. (**D**) Colocalization of the cytoplasmic 8-oxoG IR and TFAM IR. Scale bar: 10 μm. (**E**) Significantly increased mitochondrial 8-oxoG IR in DKO striatum exposed to 3-NP. Scale bar: 50 μm. (**F**) Quantitative measurement of the mitochondrial 8-oxoG IR in neuron. WT (PBS, n = 4; 3-NP, n = 4); DKO mice (PBS, n = 4; 3-NP, n = 5). (**G**) Detection of ssDNA IRs in either nuclei or cytoplasm. Arrow, cytoplasmic ssDNA IR; arrowhead, nuclear ssDNA IR. Scale bar: 20 μm. (**H**) Detection of stronger nuclear 8-oxoG IR in DKO striatal microglia. Nuclear 8-oxoG IR in RNase/HCl-pretreated sections (HCl), and to a lesser extent, cytoplasmic 8-oxoG IR in RNase-pretreated sections (no HCl) were detected in microglia. Scale bars: 20 μm (upper); 50 μm (lower). In **B** and **F**, data are shown as LS means ± SEM. Levels not connected with the same letter are significantly different (Tukey's HSD test). *P, compared with WT mice exposed to 3-NP.

Calpain as well as PARP inhibitors suppress striatal neurodegeneration and improve behavioral impairments induced by 3-NP. We next tested whether inhibition of calpain and PARP could afford neuroprotection against the neurodegeneration following 3-NP administration, to confirm the involvement of the 2 distinct pathways in 3-NP–induced neurodegeneration.

We examined the effects of administration of a calpain inhibitor (MDL28170) and an inhibitor of PARP (3-aminobenzamide [3-AB]) on striatal degeneration induced by 3-NP. Both inhibitors significantly improved 3-NP–induced motor impairments (Figure 6A) and suppressed MSN loss (Figure 6, B and C) as well as microgliosis (Figure 6D) in *Mth1/Ogg1*-DKO mice. The perinuclear distribution of α-spectrin was suppressed by the calpain inhibitor (Figure 6E), while accumulation of both PAR polymer and nuclear AIF was efficiently suppressed by the PARP inhibitor (Figure 6F). Thus, both calpain activation in MSNs and poly(ADP-ribosyl)ation causing nuclear translocation of AIF in microglia play important roles in 3-NP–induced striatal degeneration. Previous research has shown that downregulation of PARP in microglia protects neurons from secondary damage as well as preventing microgliosis following N-methyl-D-aspartate-induced hippocampal injury (39), as we observed for 3-NP–induced striatal degeneration (Figure 6C).

3-NP causes early accumulation of SSBs in mtDNA accompanied by calpain activation in striatal MSNs and delayed accumulation of SSBs in nDNA followed by activation of the PARP/AIF pathway in striatal microglia. Buildup of SSBs in either mtDNA or nDNA was found in *Mth1/Ogg1*-DKO striatum after exposure to 3-NP (Figure 3G). SSBs in nDNA are recognized by PARP, thus facilitating their repair or inducing nuclear translocation of AIF if SSBs are accumulated beyond the repair capacity, while buildup of excessive SSBs in mtDNA is known to cause mitochondrial dysfunction followed by calpain activation (34). We therefore examined the time course and spatial distribution of ssDNA IRs in comparison with those of α-spectrin or PAR IRs in DKO mice after exposure to 3-NP to delineate their interrelation.

LSCIM with an anti-ssDNA antibody revealed that IR for cytoplasmic ssDNA was prominent in the *Mth1/Ogg1*-DKO striatum in comparison with WT mice after 4 days of 3-NP exposure, while nuclear IR for ssDNA was more dominant in the striatal region where MSNs were largely lost after 7 days of 3-NP exposure (Figure 7, A and B). PAR IR was detected only in the DKO striatum exposed to 3-NP for 7 days and mostly colocalized with nuclear ssDNA IR (Figure 7C). On the other hand, cytoplasmic ssDNA IR was detected in neurons with perinuclear α-spectrin IRs (Figure 7D). These observations strongly suggest that 8-oxoG accumulated in either mtDNA in MSNs or nDNA in microglia causes accumulation of SSBs in each type of DNA, and that accumulation of SSBs in mtDNA results in calpain activation in MSNs, while that in nDNA activates the PARP/AIF pathway in microglia.

MUTYH deficiency renders mice resistant to the mitochondrial neurotoxicity of 3-NP. We previously demonstrated that MUTYH-dependent base excision repair (BER) is responsible for the accumulation of SSBs in nDNA or mtDNA with increased 8-oxoG accumulation in *Ogg1*-KO cells (34). To analyze the function of MUTYH in the striatum, we next examined the expression of MUTYH protein in striatum (Figure 8A) and found that MUTYH IR was preferentially localized to the cytoplasm and mitochondria and to a lesser extent nuclei in MSNs (Figure 8, B and C), while nuclear MUTYH IR in microglia was more apparent than that in MSNs (Figure 8D).

When we challenged *Mutyh*-KO mice with various doses of 3-NP (120 mg/kg/d to 180 mg/kg/d), we found that *Mutyh*-KO mice exhibit higher survival rates than do WT mice within 7 days of exposure (data not shown). 3-NP–induced motor symptoms were evaluated in WT and *Mutyh*-KO mice after exposure to 3-NP (150 mg/kg/d) (Supplemental Figure 6), and WT mice exhibited higher scores than did *Mutyh*-KO mice. Furthermore, we examined motor function of the survivors in the open-field test (Figure 8E). *Mutyh*-KO mice exhibited significantly better rearing performance after exposure to 3-NP (120 mg/kg/d) than did WT. Electron microscopic examination and histochemical detection of cytochrome *c* oxidase activity revealed that mitochondrial structure and function were well maintained in the *Mutyh*-KO striatum after 3-NP exposure, while mitochondria in the WT striatum were largely degenerated and exhibited lower cytochrome *c* oxidase activity than did those in the *Mutyh*-KO striatum (Figure 8, F and G), indicating that MUTYH enhances neurodegeneration.

MUTYH-initiated BER mediates 3-NP–induced neurodegeneration. We previously reported that exposure to sodium nitroprusside causes cell death accompanied by 8-oxoG accumulation in the mtDNA of quiescent MTH1-null cells and that knockdown of MUTYH in quiescent MTH1-null cells significantly prevents cell death (40). Considering this finding together with the *Mutyh*-KO phenotype, it is reasonable to assume that striatal degeneration accompanied by calpain and PARP/AIF pathways in *Ogg1*-KO or *Ogg1/Mth1*-DKO mice may be rescued by MUTYH deficiency. Because *Ogg1/Mth1/Mutyh*–triple KO mice are highly susceptible to spontaneous tumorigenesis within 100 days after birth (our unpublished observation), we tested our hypothesis using *Ogg1*-KO and *Ogg1/Mutyh*-DKO mice. *Ogg1/Mutyh*-DKO mice exhibited significantly better motor performance than did *Ogg1*-KO mice after exposure to 3-NP for 7 days (Figure 9A), and neither MSN loss nor microgliosis was evident in the DKO striatum (Figure 9, B and C). IR for nuclear and cytoplasmic ssDNA was again evident in the *Ogg1*-KO striatum after exposure to 3-NP; however, there was no such IR in the *Ogg1/Mutyh*-DKO striatum (Figure 10, A and B). In the *Ogg1*-KO striatum, cytoplasmic ssDNA

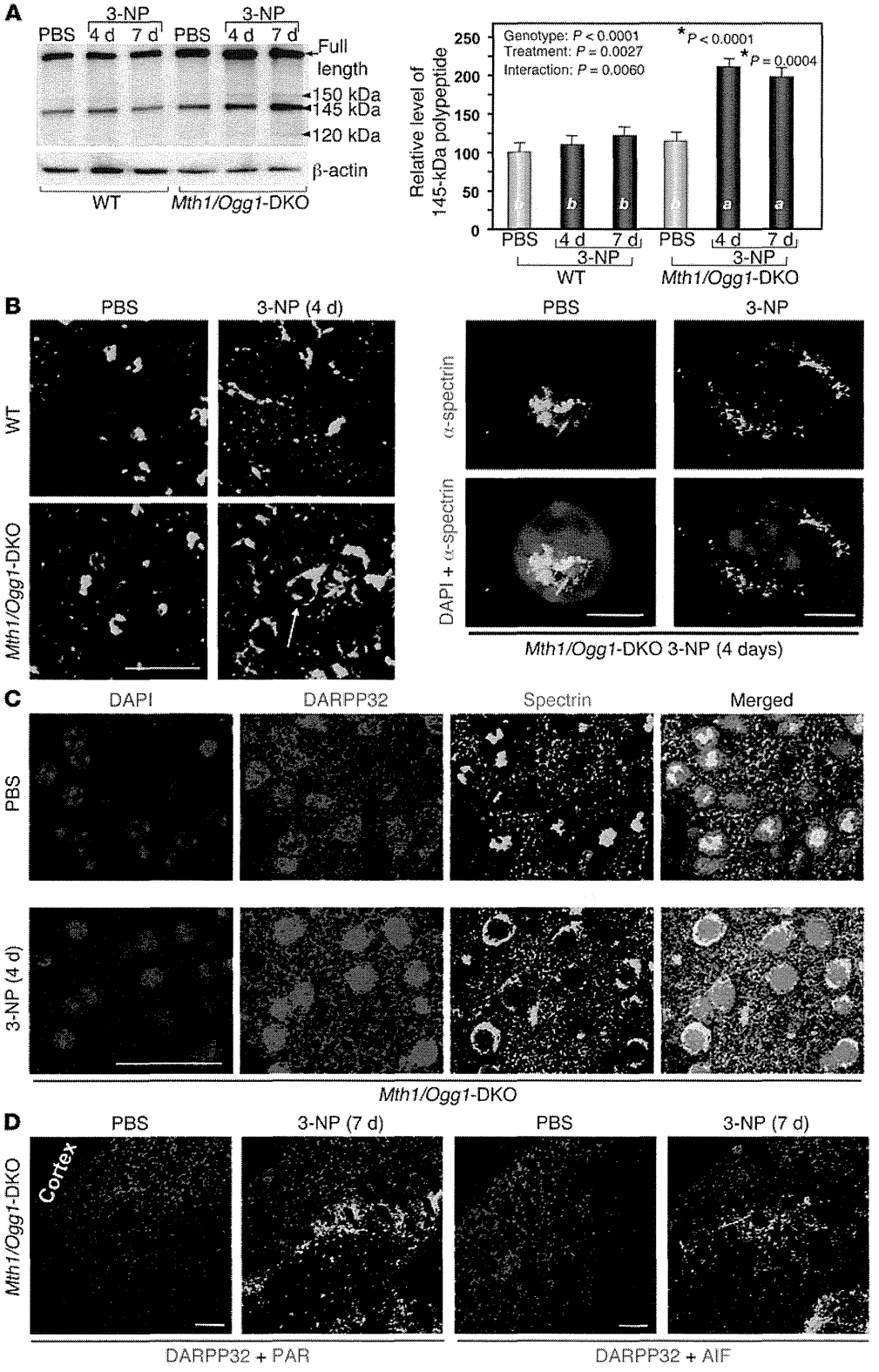

Figure 4
3-NP induces striatal degeneration dependent on calpain or PARP-AIF in *Mth1/Ogg1*-DKO mice. (**A**) Enhanced cleavage of α-spectrin by calpain in DKO striatum. Relative levels of the 145-kDa polypeptides are shown in the bar graph (right) (n = 3). Data are shown as LS means ± SEM. Levels not connected with the same letter are significantly different (Tukey's HSD test). *P, compared with the corresponding WT samples. (**B**) Altered localization of α-spectrin on the fourth day of 3-NP exposure in the DKO striatum. Localization of α-spectrin signal was changed after 3-NP exposure (arrow) (left). Scale bar: 50 μm. Magnified image showing the change of signal from nuclear to perinuclear localization (right). Scale bar: 5 μm. (**C**) Perinuclear localization of α-spectrin is evident in MSNs in the DKO striatum after 3-NP exposure. Scale bar: 25 μm. (**D**) Increased IRs for PAR and AIF in the DKO striatum where MSNs were largely depleted after 3-NP exposure. Scale bar: 50 μm.

IR was evident in DARPP32-positive neurons, while nuclear ssDNA IR was detected in F4/80-positive microglia (Figure 10, C and D) and cytoplasmic ssDNA IR was colocalized with TFAM IR after exposure to 3-NP for 7 days (Figure 10E). Moreover, we confirmed that cytoplasmic α-spectrin IRs and nuclear PAR IR were detected only in the *Ogg1*-KO but not the *Ogg1/Mutyh*-DKO striatum after exposure to 3-NP, as seen in *Mth1/Ogg1*-DKO mice (data not shown).

Finally, we confirmed that *Ogg1/Mutyh*-DKO mice exhibit resistance to 3-NP–induced locomotor dysfunction similar to that of *Mutyh*-KO mice (Supplemental Figure 7).

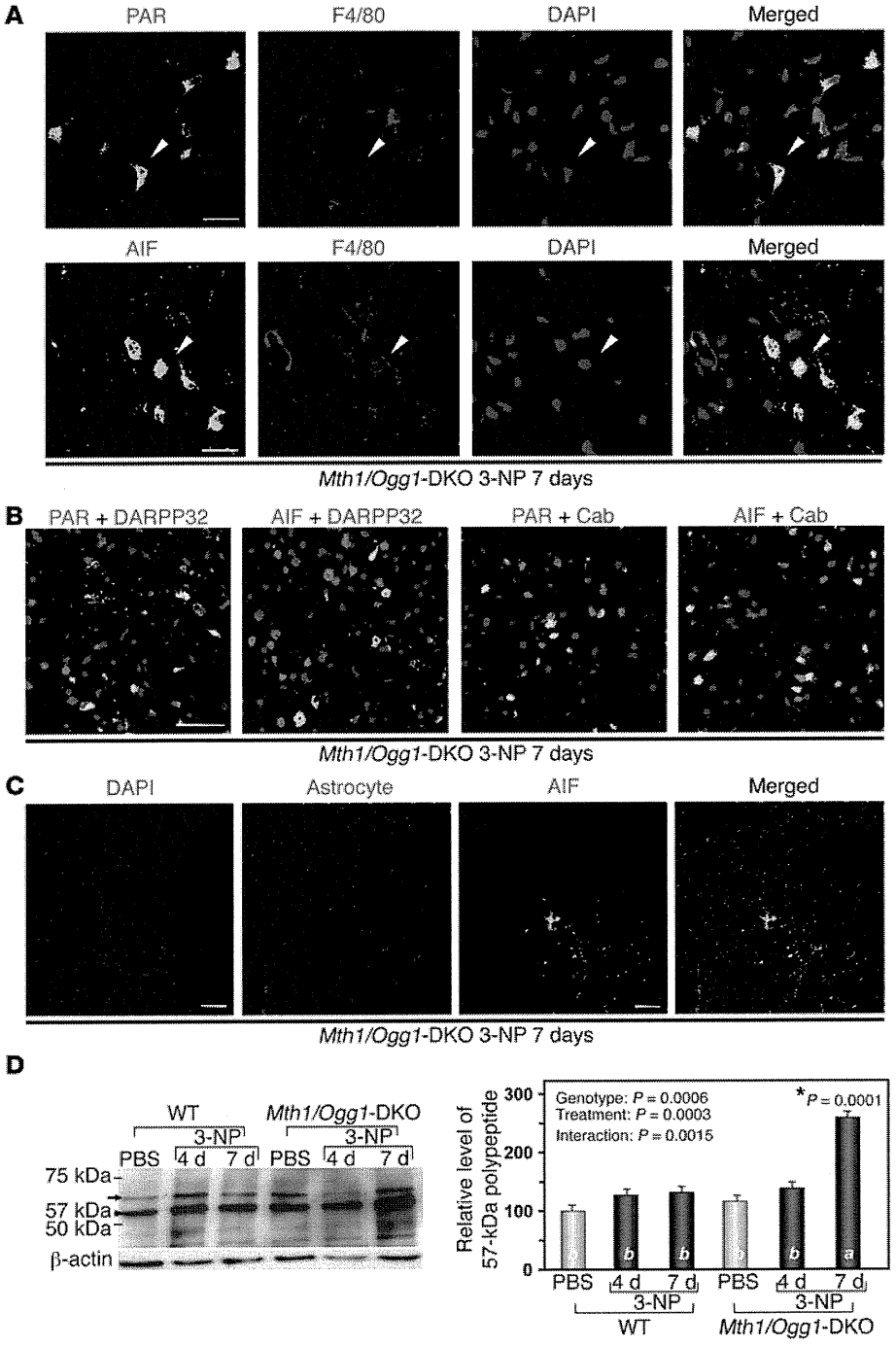

Figure 5
3-NP induces PAR and AIF accumulation in striatal microglia in *Mth1/Ogg1*-KDO mice. (**A**) Microglia in the DKO striatum exhibited IRs for PAR/AIF. Scale bars: 20 μm. (**B**) PAR and AIF were not accumulated in MSNs after 3-NP exposure. PAR/AIF, DARPP32 and calbindin (Cab), and DAPI were detected. Scale bar: 50 μm. (**C**) AIF was not accumulated in astrocytes. Scale bar: 50 μm. (**D**) 3-NP enhanced processing of AIF in DKO striatum. A 67-kDa mitochondrial form of AIF (arrow) and a 57-kDa nuclear form (arrowhead) are shown (left). Relative levels of the 57-kDa polypeptides are shown in a bar graph (right) ($n = 3$). In **D**, data are shown as LS means ± SEM. Levels not connected with the same letter are significantly different (Tukey's HSD test). *P, compared with the corresponding WT samples.

Taken together, these results indicate that 3-NP–induced striatal degeneration is largely dependent on MUTYH function under conditions of OGG1 deficiency as well as MTH1/OGG1 deficiency.

Discussion

In the present study, we demonstrated that 8-oxoG accumulated within mtDNA and nDNA under conditions of oxidative stress is differentially involved in neurodegeneration through activation of the calpain and PARP/AIF pathways. MTH1 and OGG1, which prevent accumulation of 8-oxoG in the respective DNAs, protect the brain, while MUTYH, which initiates excision repair of adenine opposite 8-oxoG, triggers neurodegeneration.

We thus propose that the neurotoxicity of oxidative stress in the mammalian brain predominantly results from MUTYH-initiated excision repair of adenine opposite 8-oxoG, which is mostly derived from 8-oxo-dGTP accumulated in the nucleotide pool under oxidative stress.

MTH1 and OGG1 suppress neurodegeneration as well as mutagenesis and carcinogenesis by preventing accumulation of 8-oxoG in cellular DNAs. It has been widely accepted that both degenerative diseases and cancers are tightly associated with

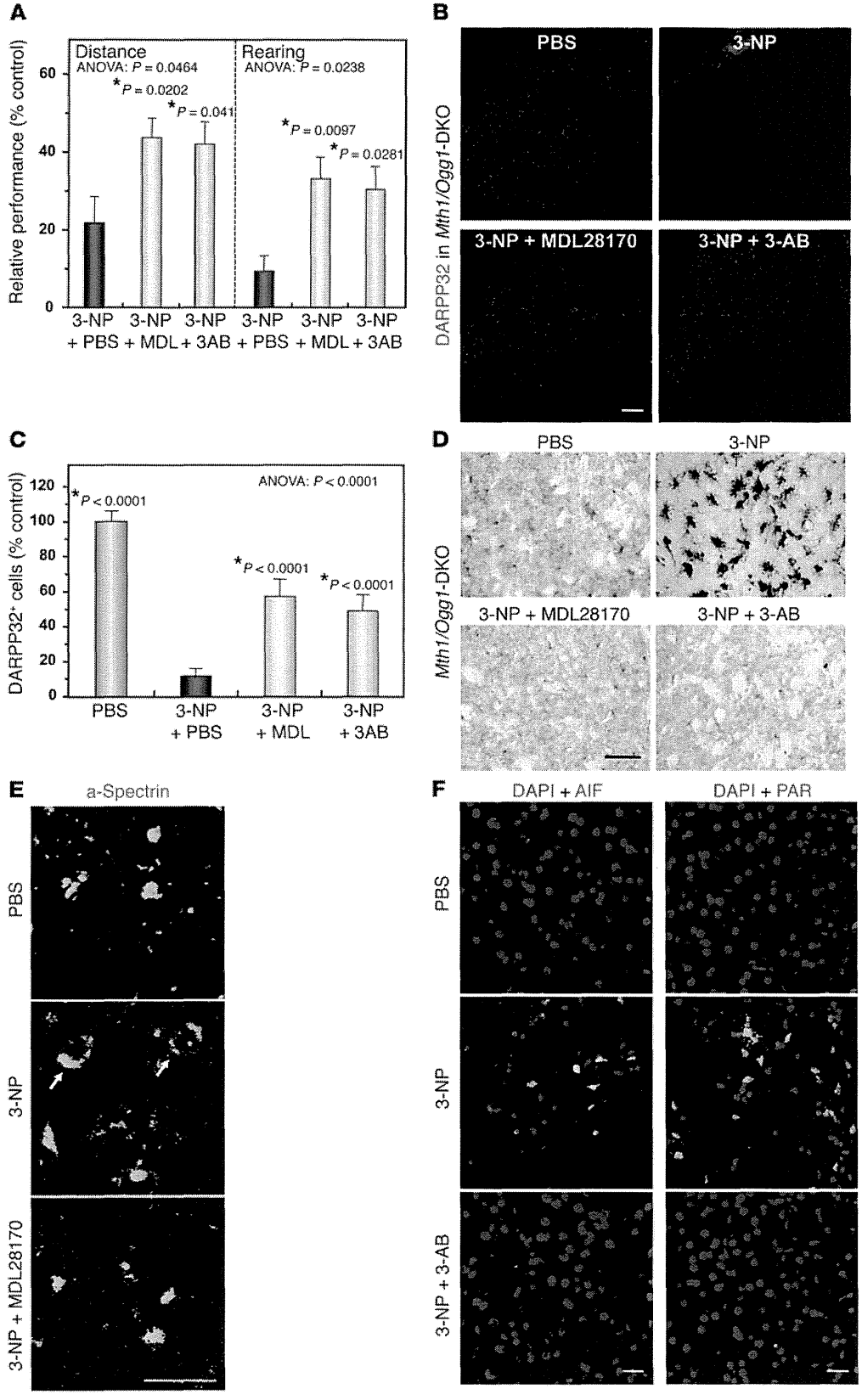

Figure 6

Calpain and PARP inhibitors suppress striatal degeneration and improve motor impairments in *Mth1/Ogg1*-DKO mice induced by 3-NP. (**A**) MDL-28170 (MDL), a cell-permeable calpain inhibitor, and 3-AB, an inhibitor of PARP, efficiently prevented 3-NP–induced motor impairments in DKO mice. Numbers of animals examined per condition are 7 (3-NP + PBS), 6 (3-NP + MDL), and 9 (3-NP + 3AB). (**B**) MDL or 3-AB suppressed loss of MSNs by 3-NP. DARPP32-positive cells (red) were detected. Scale bar: 50 μm. (**C**) MDL and 3-AB significantly suppressed loss of DARPP32-positive cells by 3-NP. Numbers of animals examined per condition are 4 (PBS), 4 (3-NP + PBS), 6 (3-NP + MDL), and 6 (3-NP + 3AB). Data are shown as LS means ± SEM. (**D**) MDL or 3-AB effectively diminished microgliosis. F4/80-positive cells (dark blue) were detected. Scale bar: 50 μm. (**E**) Calpain inhibitor inhibits perinuclear distribution of α-spectrin. Arrows, altered localization of α-spectrin. Scale bar: 50 μm. (**F**) The PARP inhibitor suppresses PAR/AIF. Scale bar: 50 μm. In **A** and **C**, the results of 1-way ANOVA are shown. **P*, compared with 3-NP + PBS (Hsu's MCB test).

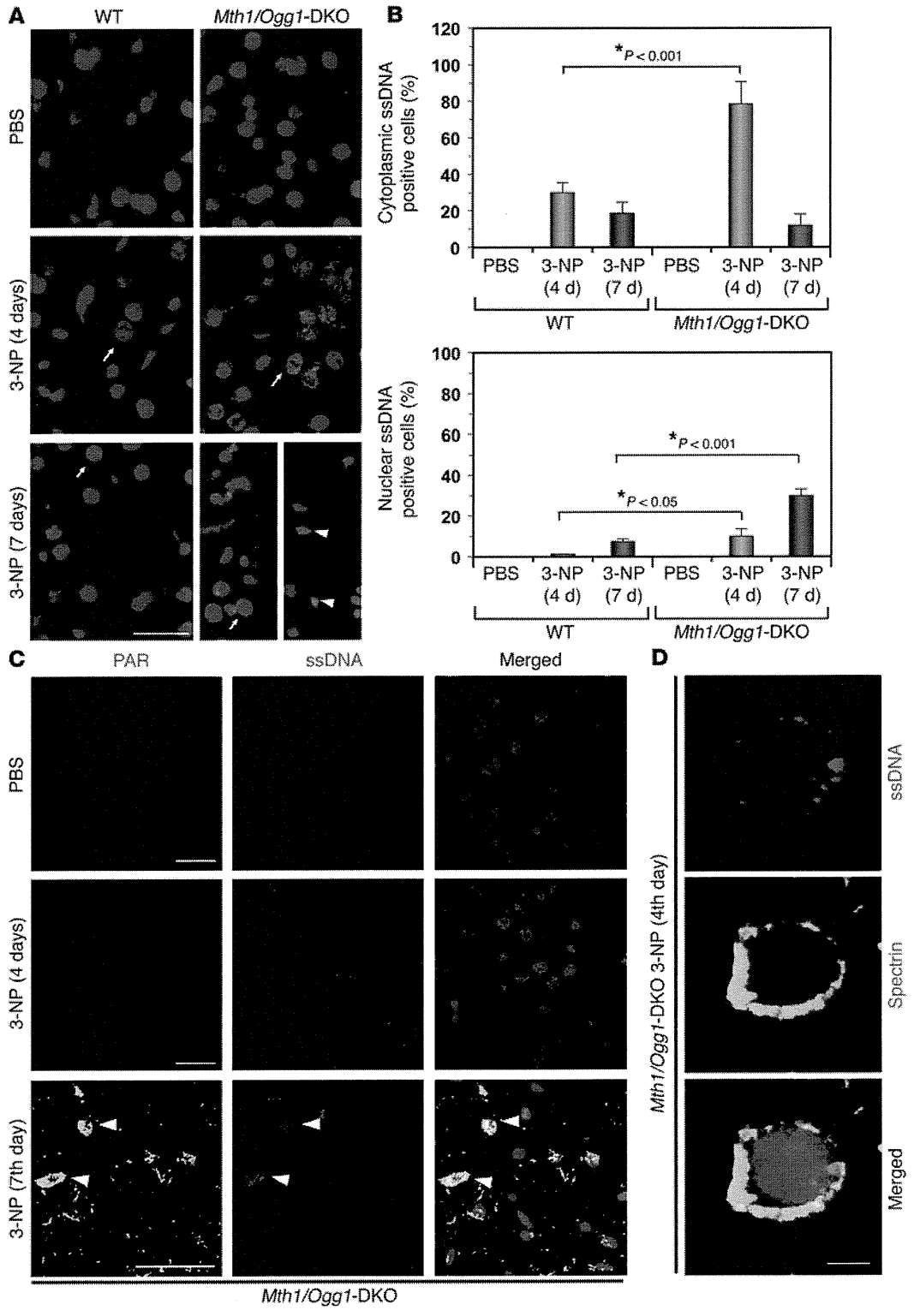

Figure 7
3-NP significantly increases accumulation of ssDNA with a delayed increase in poly(ADP-ribosyl)ation in the *Mth1/Ogg1*-DKO striatum. (**A**) Detection of ssDNA in striatum exposed to 3-NP. Strong cytoplasmic ssDNA IR was heavily detected in the *Mth1/Ogg1*-DKO striatum on the fourth day, whereas nuclear ssDNA IR was mostly seen in the DKO striatum on the seventh day, especially in the dorsolateral striatum where MSNs were lost. Arrows, cytoplasmic ssDNA+DAPI; arrow heads, nuclear ssDNA+DAPI. Scale bar: 50 μm. (**B**) The percentages of cells showing positive cytoplasmic and nuclear ssDNA IR in dorsolateral striatum were counted. The numbers of animals examined per condition are WT PBS ($n = 4$), 3-NP 4 days ($n = 4$), 3-NP 7 days ($n = 3$), DKO mice ($n = 4$) for each group. Data are shown as LS means ± SEM. (**C**) PAR IR detected in nuclear ssDNA-positive cells in DKO striatum on the seventh day of 3-NP exposure. Note that PAR IR was only detected on the seventh day, and was mostly colocalized with nuclear ssDNA IR (arrowheads). Scale bar: 50 μm. (**D**) Cytoplasmic ssDNA IR was detected in cytoplasmic α-spectrin–positive cells in DKO striatum after 3-NP exposure (fourth day). Scale bar: 5 μm.

DNA damage (1, 4). We previously showed that *Mth1*-KO and *Ogg1*-KO mice exhibit increased incidence of spontaneous tumors in liver and lung, respectively. This was accompanied by accumulation of 8-oxoG in their nDNAs, thus demonstrating that MTH1 and OGG1 prevent accumulation of 8-oxoG in nDNA, thereby suppressing mutagenesis and carcinogenesis (12, 13). However, we also found that mice lacking both MTH1 and OGG1 developed no lung tumors, although 8-oxoG was highly accumulated in nDNA (13). This observation suggests that excess accumulation of 8-oxoG under combined deficiency of MTH1 and OGG1 may induce tumor cell death, thereby leading to diminished occurrence of lung tumors (41). Furthermore,

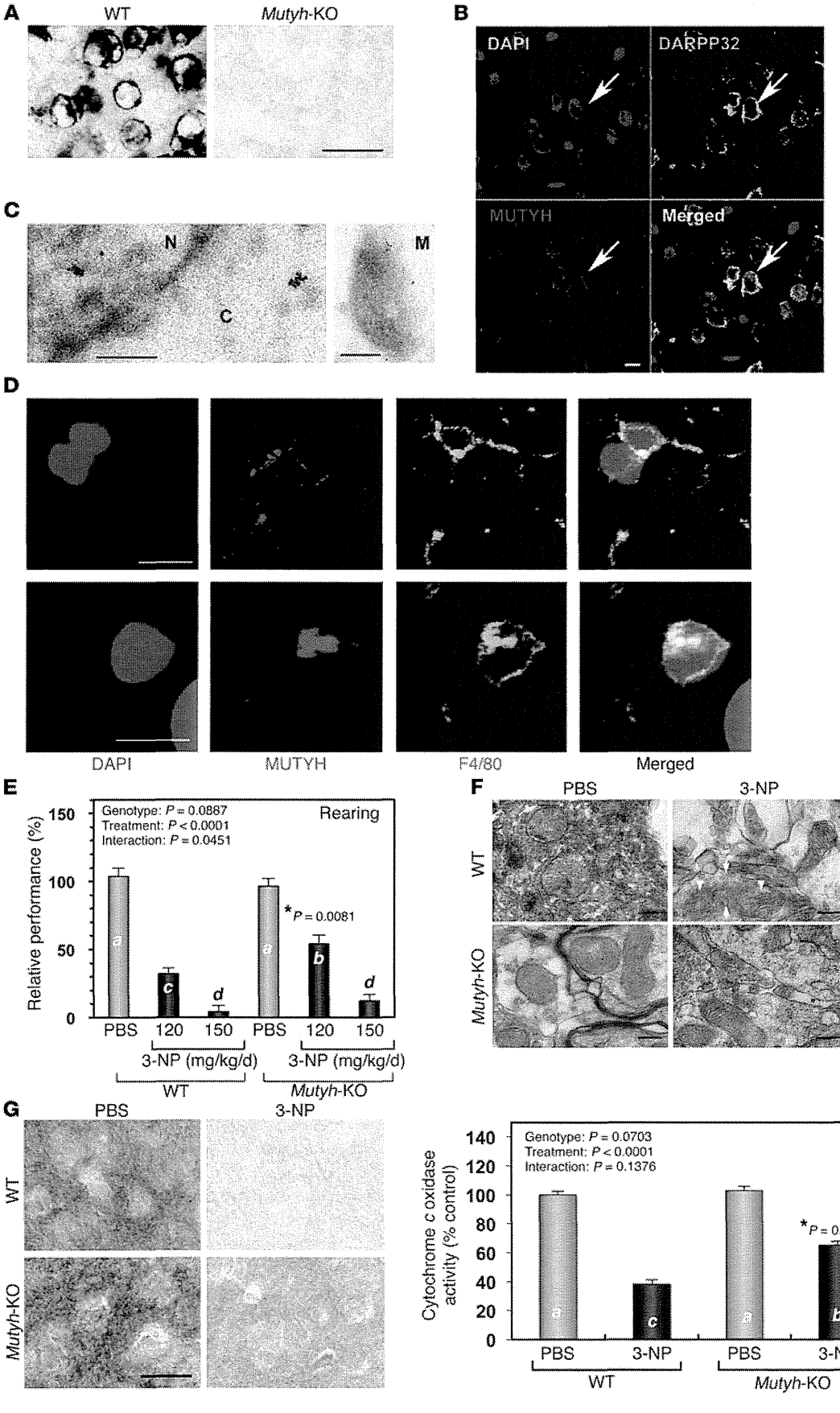
A
WT
Mutyh-KO
B
DAPI
DARPP32
MUTYH
Merged
C
N
C
M
D
DAPI
MUTYH
F4/80
Merged
E
Genotype: P = 0.0887
Treatment: P < 0.0001
Interaction: P = 0.0451
Rearing
Relative performance (%)
150
100
50
0
*P = 0.0081
a
c
d
a
b
d
PBS
120
150
PBS
120
150
3-NP (mg/kg/d)
3-NP (mg/kg/d)
WT
Mutyh-KO
F
PBS
3-NP
WT
Mutyh-KO
G
PBS
3-NP
WT
Mutyh-KO
Cytochrome c oxidase activity (% control)
140
120
100
80
60
40
20
0
Genotype: P = 0.0703
Treatment: P < 0.0001
Interaction: P = 0.1376
*P = 0.0228
a
c
a
b
PBS
3-NP
PBS
3-NP
WT
Mutyh-KO

Figure 8
Mutyh-KO mice are resistant to 3-NP–induced motor impairment and mitochondrial degeneration. (**A**) Expression of MUTYH in mouse striatum. MUTYH IRs were detected in WT but not *Mutyh*-KO brains. Scale bar: 25 μm. (**B**) MUTYH IRs were mostly detected in cytoplasm of DARPP32-positive cells in WT striatum. Scale bar: 10 μm. (**C**) Immunoelectron microscopy for MUTYH in WT striatum. C, cytoplasm; N, nucleus; M, mitochondrion. Scale bar: 250 nm. (**D**) MUTYH IR was detected in either cytoplasm or nuclei of F4/80-positive WT microglia. Scale bar: 10 μm. (**E**) Resistance of *Mutyh*-KO mice to 3-NP–induced motor impairment. *Mutyh*-KO mice exhibited a higher incidence of rearing in the open filed test after 3-NP exposure for 7 days than did WT mice. WT (PBS, $n = 6$; 3-NP 120 mg/kg/d, $n = 10$; 3-NP 150 mg/kg/d, $n = 10$); *Mutyh*-KO (PBS, $n = 7$; 3-NP 120 mg/kg/d, $n = 5$; 3-NP 150 mg/kg/d, $n = 10$). (**F**) Mitochondrial degeneration in striatum induced by 3-NP. Electron microscopy revealed disruption of outer and inner membranes (arrows) and cristae (arrowheads) in striatal mitochondria of WT but not *Mutyh*-KO mice (3-NP, 150 mg/kg/d, for 7 days). Scale bar: 200 nm. (**G**) Mitochondrial function was maintained in *Mutyh*-KO mice after 3-NP administration. Mitochondrial function was examined by histochemical detection of cytochrome oxidase activity. Images were obtained by DIC microscopy. WT (PBS, $n = 4$; 3-NP, $n = 4$); *Mutyh*-KO (PBS, $n = 5$; 3-NP, $n = 5$). Scale bar: 20 μm. In **E** and **G** (right), data are shown as LS means ± SEM. Levels not connected with the same letter are significantly different (Student's *t* test). **P*, compared with the corresponding WT sample.

we have shown that increased accumulation of 8-oxoG in nDNA and/or mtDNA causes cell death and that MTH1 and OGG1 suppress cell death (34, 40, 42).

We previously reported that *Mth1*-KO mice exhibit increased accumulation of 8-oxoG in the mtDNA of striatal nerve terminals of dopamine neurons after 1-methyl-4-phenyl-1,2,3,6-tetrahydropyridine administration, followed by more severe terminal degeneration of dopamine neurons in comparison to WT mice (31). MTH1 also efficiently suppresses the accumulation of 8-oxoG in mtDNA in the hippocampus caused by kainate-induced excitotoxicity, especially in microglia (43). Moreover, it has been shown that human MTH1 transgenic mice are resistant to 3-NP–induced striatal degeneration (27), suggesting that increased accumulation of 8-oxoG in brain causes neurodegeneration.

In the present study, we showed that double deficiency of MTH1 and OGG1 renders the striatum highly vulnerable to 3-NP–induced neurodegeneration, accompanied by highly increased accumulation of 8-oxoG in both the mtDNA of MSNs and the nDNA of microglia in the striatum. This is the first experimental evidence that OGG1 and MTH1 cooperatively suppress 8-oxoG accumulation in brain DNAs, thus protecting the brain from neuronal loss and microgliosis, which result in severe neurodegeneration and behavioral impairments.

Mitochondria prepared from caudate nucleus as well as other regions of mouse brain possess substantial levels of OGG1 incision activity (44). In the present study, we found that OGG1 was predominantly localized in the mitochondria of MSNs in normal striatum (Figure 1A) and that OGG1 deficiency significantly increased accumulation of mitochondrial 8-oxoG and ssDNA in MSNs after exposure to 3-NP. Considering these findings together, we concluded that mitochondrial OGG1 is crucial to protect striatal MSNs from oxidative stress.

MUTYH suppresses carcinogenesis but promotes neurodegeneration by inducing cell death. We have shown that *Mutyh*-KO mice exhibit the most significant increase in spontaneous occurrence of tumors among *Mth1*-, *Ogg1*-, and *Mutyh*-KO mice (14). It has been reported that *Ogg1/Mutyh*-DKO mice (15) and *Mth1/Ogg1/Mutyh*–triple-KO mice exhibit markedly increased spontaneous tumorigenesis in various tissues over a much shorter period (our unpublished observations). These observations indicate that MUTYH functions as the strongest suppressor of tumorigenesis among the 3, because *Mth1/Ogg1*-DKO mice develop no lung tumors whereas *Ogg1*-KO mice do (13). Thus, we hypothesized that MUTYH induces cell death, thereby suppressing tumorigenesis in the absence of MTH1 and OGG1. We previously showed that MUTYH is required for generation of SSBs in DNA and induction of cell death when 8-oxoG is highly accumulated in either nDNA or mtDNA under conditions of oxidative stress (34, 40, 41).

In the present study, we found that MUTYH protein is highly expressed in the striatum and is mostly present in the mitochondria of MSNs and that *Ogg1/Mutyh*-DKO mice exhibit markedly increased resistance to 3-NP–induced striatal degeneration in comparison with *Ogg1*-KO mice and even WT mice. These results clearly demonstrate that MUTYH enhances neurodegeneration through the induction of cell death once 8-oxoG becomes accumulated in neurons and/or microglia.

MUTYH-initiated BER induces accumulation of SSBs in DNA, thereby triggering 2 distinct cell death pathways dependent on calpain or PARP-AIF. We previously established that MUTYH initiates the 2 distinct pathways of cell death while 8-oxoG accumulates selectively in mtDNA or nDNA in *Ogg1*-KO cell lines (34). In the present study, we found that 8-oxoG is significantly accumulated first in the mtDNA of MSNs ($P < 0.0001$) and then in the nDNA of microglia during striatal degeneration caused by 3-NP in the absence of OGG1 and/or MTH1. This is followed by selective accumulation of SSBs in each type of DNA. Calpain activation was observed in MSNs, while nuclear accumulation of PAR-polymer and AIF was evident in microglia. Calpain activation, PARP-AIF activation, and accumulation of SSBs were observed in *Ogg1*-KO mice, but were efficiently suppressed by a lack of MUTYH, which initiated BER of adenines inserted opposite 8-oxoG (41). Moreover, administration of inhibitors of calpain or PARP to *Mth1/Ogg1*-DKO mice efficiently suppressed 3-NP–induced loss of MSNs and microgliosis in the striatum, and this was followed by improvement of motor impairment. Considering these observations together, we concluded that MUTYH-initiated BER induces accumulation of SSBs in DNA, thereby triggering 2 distinct cell death pathways dependent on calpain or PARP-AIF, as summarized in Figure 11. The anti-ssDNA antibody used in the present study also recognizes single-stranded regions of double-stranded breaks (DSBs) generated by resection of the ends (45). It is thus possible that DSBs may also be generated through incision of the template strand if there are other types of damaged bases close to 8-oxoG in the template DNA generated under increased oxidative stress.

Recently, Foti et al. reported that cytotoxicity of bactericidal antibiotics such as β-lactams and quinolones predominantly results from lethal double-strand DNA breaks caused by incomplete repair of closely spaced 8-oxoG lesions and is efficiently suppressed by *mutM/mutY*-double deficiency (5). Considered together with our previous findings (28, 34, 40–42), it is noteworthy that 8-oxoG accumulated in the genome causes cell death through a common mechanism from bacteria to mammals. In the mammalian brain, however, there are different types of cells, such as neurons and microglia, and each cell has 2 distinct genomes, 1 in the nucleus, and 1 in mitochondria. Our findings in the present study

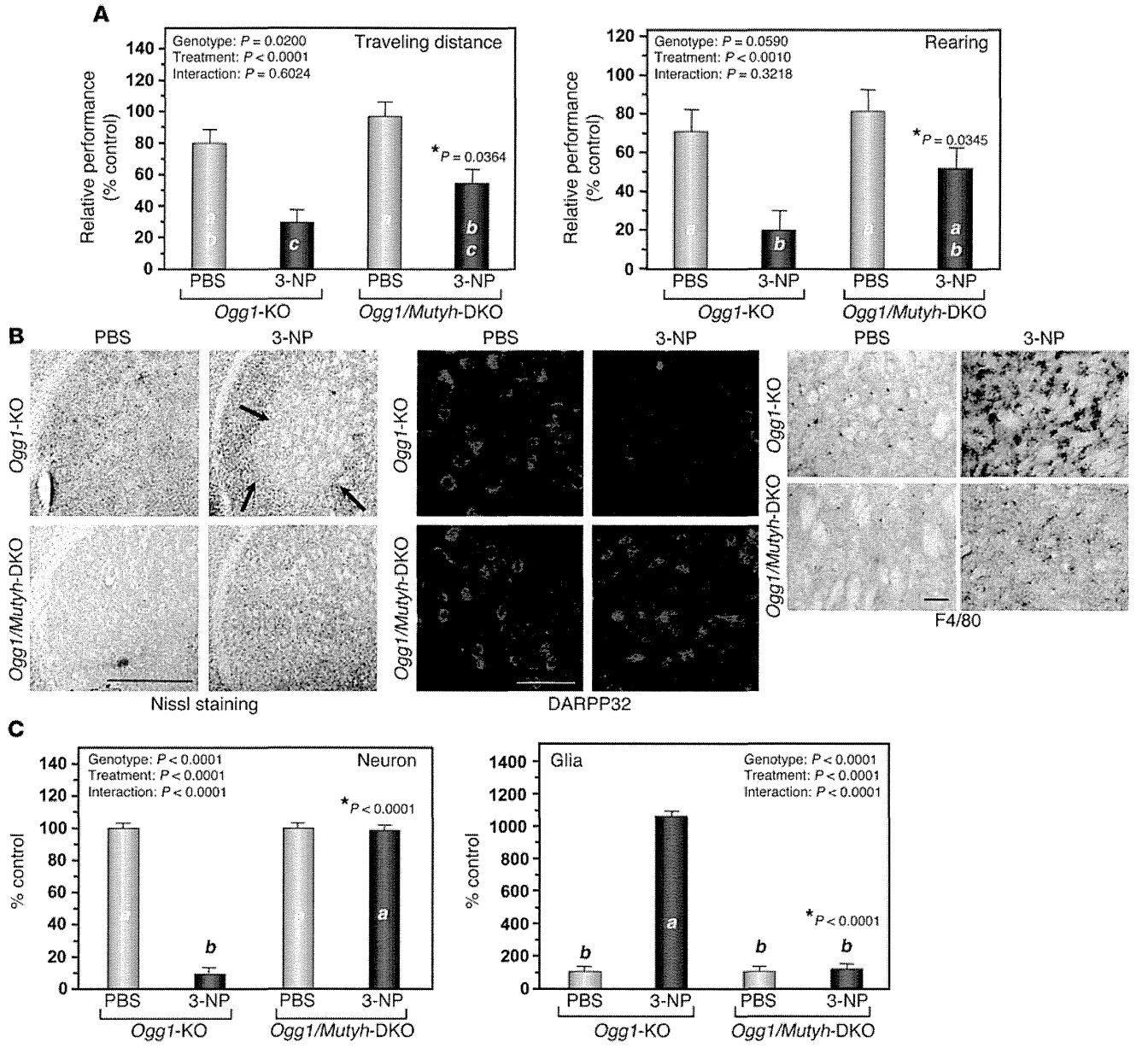

Figure 9

MUTYH deficiency ameliorates 3-NP–induced motor impairments and striatal degeneration in *Ogg1*-KO mice. (**A**) MUTYH deficiency ameliorates 3-NP–induced motor impairments in *Ogg1*-KO mice. *Ogg1/Mutyh*-DKO mice exhibited better performances in the open-field test after exposure to 3-NP for 7 days than did *Ogg1*-KO mice. *Ogg1*-KO (PBS, $n = 7$; 3-NP, $n = 8$); *Ogg1/Mutyh*-DKO (PBS, $n = 6$; 3-NP, $n = 7$). (**B**) MUTYH deficiency suppresses striatal degeneration. Nissl staining (left panels). DARPP32-positive MSNs (center panels). F4/80-positive microglia (3,3′-diaminobenzidine/nickel staining, right panels). Scale bar: 1 mm (left); 50 μm (center); 50 μm (right). (**C**) The numbers of neurons and glial cells in the dorsolateral striatum with or without 3-NP exposure for 7 days. Cells were counted in Nissl-stained sections, $n = 3$ for each group. Data are shown as LS means ± SEM. Levels not connected with the same letter are significantly different. **P*, compared with *Ogg1*-KO mice exposed to 3-NP.

show for what we believe is the first time that neurodegeneration is a complex process caused by 8-oxoG accumulated in the 2 distinct genomes in the brain.

Neurodegeneration induced by 8-oxoG and MUTYH depends on both replication of mtDNA in neurons and nDNA in microglia. Overexpression of human MTH1 in mouse striatum efficiently abrogates 3-NP–induced striatal degeneration accompanied by effective suppression of 8-oxoG accumulation in the striatum (27). *Mth1/Ogg1*-DKO mice exhibited the highest susceptibility to 3-NP–induced striatal degeneration with the highest levels of 8-oxoG in striatal DNAs. These findings indicate that the major source of 8-oxoG accumulated in DNA are 8-oxo-dGTP generated in nucleotide pool; the former is repaired by OGG1 and the latter is hydrolyzed by MTH1.

DNA replication is essential for accumulation of 8-oxoG in the respective DNA; moreover, insertion of adenine opposite 8-oxoG also depends on replication. Neurons are postmitotic and only mtDNA but not nDNA is always replicated in neurons in order

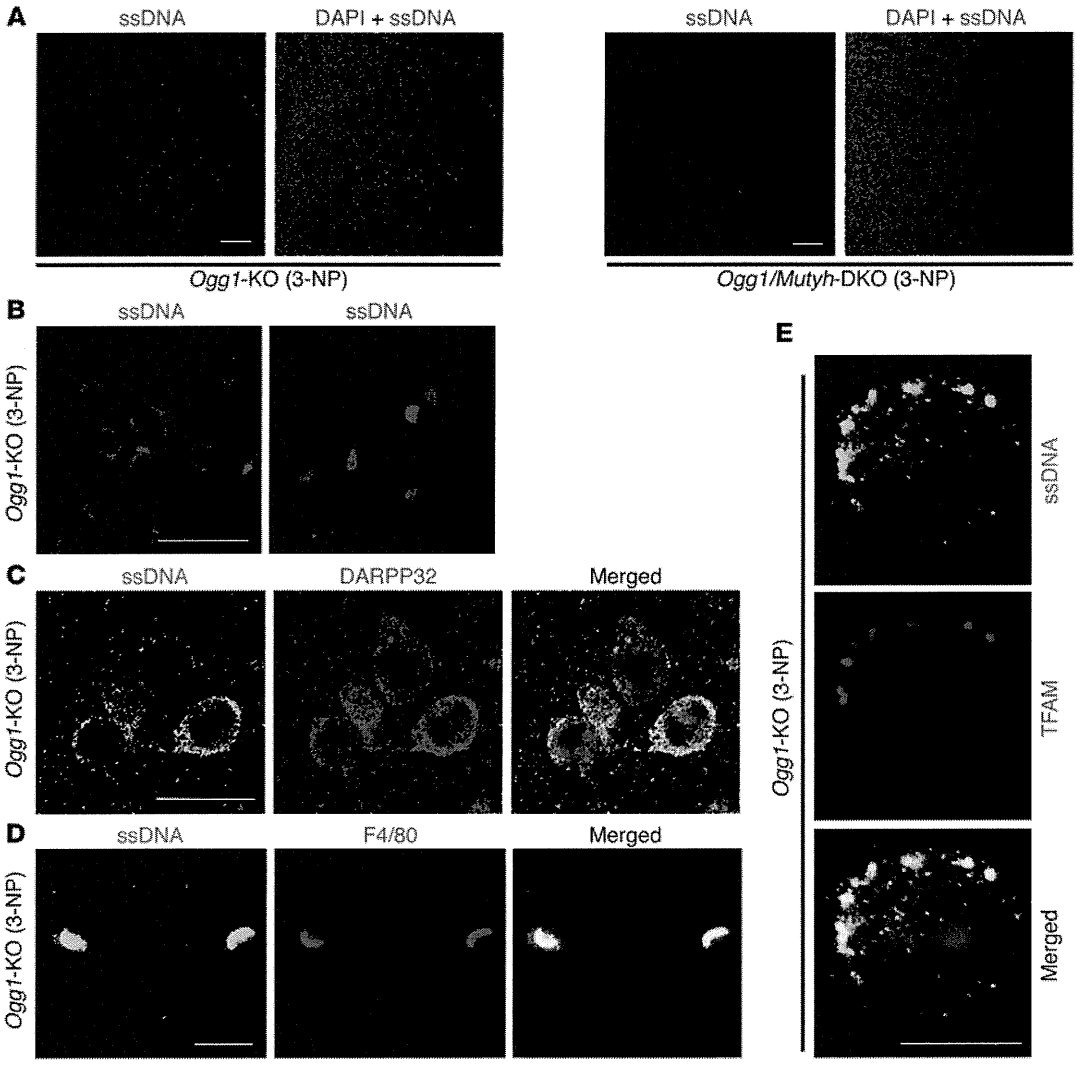

Figure 10
MUTYH deficiency suppresses both nuclear and mitochondrial ssDNA accumulation in *Ogg1*-KO mice. (**A**) ssDNA accumulation was only found in *Ogg1*-KO mice after exposure to 3-NP for 7 days. Scale bar: 50 μm. (**B**) Nuclear and cytoplasmic ssDNA were detected in *Ogg1*-KO mice after exposure to 3-NP for 7 days. Scale bar: 50 μm. (**C**) Cytoplasmic ssDNA IR was specifically detected in *Ogg1*-KO MSNs after exposure to 3-NP for 7 days. Scale bar: 20 μm. (**D**) Nuclear ssDNA IR was specifically detected in *Ogg1*-KO microglia after exposure to 3-NP for 7 days. Scale bar: 20 μm. (**E**) Cytoplasmic ssDNA IR was colocalized with TFAM IR in *Ogg1*-KO striatum after exposure to 3-NP for 7 days. Scale bar: 10 μm.

to provide the energy essential for maintenance of neuronal functions. 8-oxoG is therefore dominantly accumulated in mtDNA of neurons under conditions of oxidative stress, resulting in SSB accumulation in mtDNA during MUTYH-initiated BER of adenine inserted opposite 8-oxoG. In contrast, microglia are mitotic; thus, 8-oxoG and SSBs accumulated in nDNA dependent on their replication and MUTYH-initiated BER (Figure 11). Thus, replication of the respective DNAs in neurons and microglia determines which of the 2 separate signaling pathways must be activated upon accumulation of 8-oxoG under conditions of oxidative stress.

Microgliosis is a delayed event in striatal degeneration induced by 3-NP (Figure 1D); therefore, it is likely that accumulation of 8-oxoG followed by ssDNA accumulation in nDNA of microglia (Figures 3H and 7B) is not due to a direct effect of mitochondrial ROS generated in MSNs immediately after exposure to 3-NP. Neurons damaged by mitochondrial ROS thereafter induce a delayed inflammatory response, resulting in microgliosis, which is known to be accompanied by secondary generation of ROS in brain (46). Since inhibition of PARP activity, which is activated by SSBs accumulated in the nDNA of microglia resulting in AIF activation (Figure 5, A and D), efficiently suppressed neuronal loss as well as microgliosis, ROS generated in microglia may in turn attack neurons to promote the degenerative process as suggested by Brouillet et al. (36), thus initiating a vicious cycle of neurodegeneration.

Growing evidence suggests that mitochondrial dysfunction is generally associated with neurodegenerative diseases (47) and that microglial activation is also involved in the pathogenesis of most forms of neurodegeneration (48). It is known that activation of calpain, PARP, and AIF is involved in various neurodegenera-

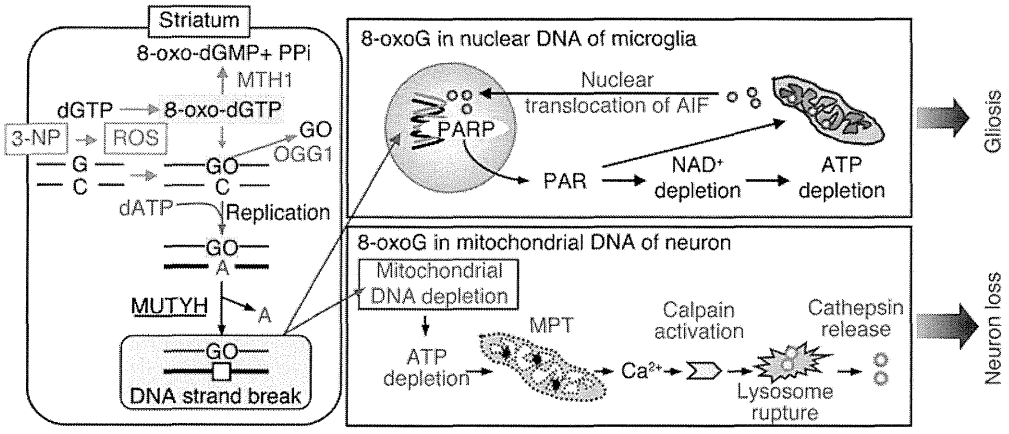

Figure 11
Molecular mechanisms underlying 8-oxoG–induced striatal degeneration. Chronic administration of the mitochondrial neurotoxin 3-NP to mutant mice lacking OGG1, which excises a major oxidative base lesion 8-oxoG (GO) opposite cytosine from DNA, and/or MTH1, which hydrolyses 8-oxo–dGTP in the nucleotide pool to prevent its harmful incorporation into DNA, causes significantly increased accumulation of 8-oxoG in the striatum. At an early stage, buildup of 8-oxoG in the mitochondrial DNA of striatal MSNs causes calpain-dependent neuronal loss triggered by mitochondrial MUTYH-initiated BER of adenines opposite 8-oxoG. In the later stages, buildup of 8-oxoG in the nuclear DNA of microglia causes PARP-dependent nuclear translocation of mitochondrial AIF triggered by nuclear MUTYH-initiated BER, thus resulting in microgliosis. Two distinct pathways of cell death, both dependent on MUTYH-initiated BER (34), result in severe striatal degeneration and motor impairments.

tive diseases such as AD, PD, and HD (38, 49), in which 8-oxoG is a common molecular marker (50), together with altered expression of MTH1, OGG1, and MUTYH (16, 19–22). Inhibition of calpain and PARP has been considered to be a potential therapeutic approach for neurologic disorders (38, 49).

Our findings in the present study show that 2 distinct molecular pathways are separately activated in the mitochondria of neurons and the nuclei of microglia through oxidative DNA damage and its repair, thus providing insights into the molecular mechanisms underlying neurodegeneration under conditions of oxidative stress as well as providing therapeutic targets for neurodegenerative diseases. Suppression of MUTYH may thus be an efficient strategy for protecting the brain under conditions of oxidative stress. However, it will be important not to increase the risk of carcinogenesis under MUTYH suppression; therefore, further experimental evaluation is essential.

Methods

Mice. We previously established *Mth1*, *Ogg1*, and *Mutyh* gene KO mice (12, 13, 51). Heterozygous mice (*Mth1*$^{+/-}$, *Ogg1*$^{+/-}$, *Mutyh*$^{+/-}$) were backcrossed to C57BL/6J mice (Clea Japan) for more than 15 generations, thereby ensuring the mice were on a pure C57BL/6J genetic background. Homozygous KO mice (*Mth1*$^{-/-}$, *Ogg1*$^{-/-}$, *Mutyh*$^{-/-}$) were generated by crossing of the corresponding heterozygous mice and inbred for 2 to 3 generations to obtain the mice used in each experiment. *Mth1*$^{+/-}$*Ogg1*$^{+/-}$ double-heterozygous mice obtained by crossing of *Mth1*$^{+/-}$ and *Ogg1*$^{+/-}$ mice were crossed to obtain *Mth1*$^{-/-}$*Ogg1*$^{-/-}$ (*Mth1*/*Ogg1*-DKO) mice and were inbred for 2 to 3 generations to obtain the mice used in each experiment. *Ogg1*$^{+/-}$*Mutyh*$^{+/-}$ double-heterozygous mice were obtained by crossing *Ogg1*$^{+/-}$ and *Mutyh*$^{+/-}$ mice to obtain *Ogg1*$^{-/-}$*Mutyh*$^{-/-}$ (*Ogg1*/*Mutyh*-DKO), and these were inbred for 2 to 3 generations to obtain the mice used in each experiment. C57BL/6J mice were used as the WT strain. All animals were maintained in an air-conditioned, specific pathogen–free room with time-controlled lighting.

Treatment with 3-NP. Ten-week-old male mice were used. 3-NP (Sigma-Aldrich) was dissolved in PBS and systemically administered via an i.p. implanted osmotic minipump (1007D, Alzet; delivering 0.5 μl/h for 7 days). All animals were subjected to surgical operations between 9:00 am and 12:00 pm. Mice were anesthetized with pentobarbital (30 mg/kg, i.p.), an incision was made in the abdomen, and the osmotic minipump was implanted into the i.p. cavity. In typical experiments, mice were exposed to 120 mg of 3-NP/kg/d for 7 days, and the control mice were subjected to implantation of the osmotic minipump containing PBS for 7 days. To compare 3-NP resistance between *Mutyh*-KO and WT mice, a higher dose of 3-NP (150 mg/kg/d) was applied.

Treatment with MDL28170 and 3-AB. A calpain inhibitor (MDL28170, Biomol) or a poly-(ADP-ribose) polymerase inhibitor (3-AB; Sigma-Aldrich) was administered together with 3-NP to *Mth1*/*Ogg1*-DKO mice. Two osmotic minipumps prefilled with 3-NP (120 mg/kg/d) and MDL28170 (50 mg/kg/d, dissolved in dimethyl sulfoxide, then diluted in PBS) or 3-AB (30 mg/kg/d, dissolved in PBS) were simultaneously implanted for 7 days. Control mice were implanted with 2 minipumps prefilled with 3-NP (120 mg/kg/d) and PBS.

Behavioral analysis. 3-NP–induced motor symptoms were evaluated using a quantitative neurological scale based on previous reports (29, 30). Neurological scores were defined as follows: score = 0, normal behavior; 1, general slowness of displacement resulting from mild hind limb impairment; 2, incoordination and marked gait abnormality; 3, hind limb paralysis; 4, incapacity to move resulting from forelimb and hind limb impairment; 5, recumbency.

Spontaneous locomotor activity in the home cage was measured using a digital counter with an infrared beam sensor (NS-ASS01; Neuroscience, Inc.), placed about 200 mm above the center of the home cage (27 × 14 × 15 cm), and analyzed using DAS-008 software.

To evaluate the extent of motor impairment induced by 3-NP exposure, an open-field test was performed. Behavioral analysis was performed between 9:00 am and 12:00 pm. A mouse was placed in the center of a circular open field (60 cm in diameter, 30 cm deep). Motor activity was quantified using an automated video tracking system, the video-image motion analyzer AXIS-90 (Neuroscience Inc.). Traveling distance and numbers of rearing behaviors were measured for 5 minutes. To avoid a reduction in motor activity due to habituation to the open field, motor activity was recorded only twice, on the day before implantation of the osmotic minipump (baseline performance) and on the seventh day after the operation. The number of animals examined is shown in each figure legend. Relative performance indicates the traveling distance or number of rearing times obtained on the seventh day after implantation of an osmotic minipump as a percentage of that obtained on the day before implantation.

Rotarod testing was performed between 9:00 am and 12:00 pm. The test was performed using an accelerating rotarod for mice (Model 7650; UGO Basile). Prior to 3-NP treatment, all mice were given 3 trials on the rotarod,